FERMILAB-MASTERS-2023-06

Improving The Simulation Of Muons In The Rock Around The NOvA Near Detector

A THESIS
SUBMITTED TO THE FACULTY OF THE GRADUATE SCHOOL
OF THE UNIVERSITY OF MINNESOTA
BY

Radwan Parvez

IN PARTIAL FULFILLMENT OF THE REQUIREMENTS
FOR THE DEGREE OF
MASTER OF SCIENCE

Dr. Alec Habig

August, 2023

Acknowledgements

I would like to offer my deepest appreciation to everyone who helped and contributed to the completion of this thesis. Their invaluable assistance and encouragement were crucial in this journey.

First and foremost, I want to express my heartfelt gratitude to my supervisor **Dr. Alec Habig** for his constant advice, knowledge, patience and encouragement during this research. His insightful ideas and guidance have been the most crucial and foundational cornerstone of this research journey. I also want to thank **Dr. Richard Gran** and **Dr. Harsh Jain** for agreeing to be on my thesis committee and providing their valuable review and advice.

I am indebted to **Jean-Marco Alameddine**, one of the influential contributor to the PROPOSAL project, to help me with technical guidance on code algorithm and to elaborate nuanced topic regarding PROPOSAL. Jean-Marco's willingness to share his knowledge and provide detailed explanations has been pivotal in enhancing my understanding of the simulation tool and its implementation.

I am deeply thankful to my friend **Md. Habib E Islam Digonto** for his invaluable support in coding during the course of this research. Digonto's expertise and dedication in programming were helpful in one very crucial moment of my research.

Lastly, my sincere thanks go to my family (my sisters **Jannatul Ferdaus**, **Jannatul Adnin**, and my Aunt **Kulsum Akter**) and friends for their unwavering love, support, and faith in me. Throughout the difficult parts of this thesis, their encouragement has been a continual source of motivation.

Dedication

To My Parents:

Peara Begum

&

A K M Abu Yousuf

Abstract

This thesis investigates the viability of the PROPOSAL lepton propagation tool as an alternative to the commonly used GEANT4 simulation for muon propagation within the NOvA experiment. The main objectives of this research were twofold: first, to validate the accuracy of PROPOSAL data in simulating rock muons when compared to GEANT4 data; second, to explore the practical application of transporting cosmic muons through the NOvA rock region using PROPOSAL. Additionally, an 1D analysis was conducted to determine the optimal altitude at which to hand over the simulation task from PROPOSAL to GEANT4, should we choose to use PROPOSAL for rock simulations and GEANT4 for detector simulations in the NOvA experiment. By thoroughly examining these aspects, this study aims to contribute to the advancement of muon simulation techniques and their implementation in high-energy experiments such as NOvA.

Contents

List of Tables

List of Figures

Chapter 1

Introduction

Scientific discovery and understanding comprise the formulation of theories to explain observed events, the planning and implementation of experiments to evaluate those theories, and the incorporation of experimental outcomes to refine and advance the theories. This process is the modern scientific method which is the bedrock of our understanding of reality scientifically. Simulation or modeling comes in between the theory and experiment in this process. A simulation tool (mainly numerous kinds of software) implements the formulas of the concerned theory and execution of the tool, which can be thought as a virtual experiment, provides results that can help us to realize, visualize, predict, optimize and many more for the concerned phenomena. Particle physicists also employ complicated computer simulations to interpret the massive amounts of data produced in particle collider experiments. Our comprehension of particle collisions, radiation patterns, decays, detector interactions, and sensor readings is aided by these simulations.

One of the widely used simulation tool for particle and nuclear physics experiment is GEANT4 [1] which is currently used in the simulation chain of Fermilab's neutrino experiment NOvA (NuMI Off-axis ν Appearance). It allows researchers to model particle passage through matter and investigate their interactions with various materials. It is a powerful and highly versatile tool that has extensive capabilities of simulating particle collisions, electromagnetic interactions, hadronic processes, optical photon transport, implementing effects of complex detector systems, visualizing, data analysis and many more.

However, despite of its robustness and accuracy, usage of GEANT4 can be a time consuming and computationally expensive endeavour for simulating large volume of particles over high energy range in dense mediums. Particularly, for the NOvA experimental setup, simulating particles through the "NOvA Rock Region", where particles have to propagate through a region of rock and soil, can be a highly time consuming process.

In addition, there are alternative simulation tools available that employ different methodologies, enabling us to accelerate our simulation processes in NOvA while preserving a substantial degree of precision and accuracy. One notable tool in this regard is PROPOSAL [2]. Unlike GEANT4, PROPOSAL has been exclusively designed to simulate the propagation of leptons within various mediums. Originally developed for neutrino experiments such as IceCube and ANTARES, which involve the passage of a large number of leptons (e.g., neutrinos) through a cubic kilometer of ice (for IceCube) and Water (for ANTARES) before reaching the detector, PROPOSAL stands out for its ability to significantly reduce computational time while maintaining a noteworthy level of accuracy. This appealing characteristic has motivated us to consider implementing PROPOSAL for simulating the lepton propagation in the rock region of NOvA experiment.

1.1 The NOvA Experiment

The NOvA (**N**uMI **O**ff-axis ν_e **A**ppearance) experiment is the flagship neutrino experiment of Fermi National Accelerator Laboratory. This experiment is designed to study the phenomena called *Neutrino Oscillation*. The standard picture for the case of neutrino is that it has 3 different types (physicists call these types flavour), naming electron-neutrino (ν_e), muon-neutrino (ν_μ) and tau-neutrino (ν_τ), each of which is a partner to its charged lepton, electron (e), muon (μ) and tau (τ) respectively. It turns out that one flavour of neutrino can transform into another flavour [3]. This phenomena of transformation is known as *Neutrino Oscillation*. The phenomena was proposed by Bruno Pontecarvo in 1968 to explain the infamous "solar neutrino" problem [4], where physicists had found that the amount of neutrinos that should come from the sun is not being detected on earth. Building upon the pioneering work of Pontecorvo,

it has been proposed that a fraction of neutrinos, such as ν_e, emanating from the Sun may undergo flavor transformation during their journey through space. Consequently, detection mechanisms designed to identify only ν_e particles might not capture these transformed neutrinos. If that is the case that if one flavor can change into another spontaneously, according to quantum mechanics it means that neither of the ν_e or ν_μ is a stationary state of the system (meaning, neither of them are eigenfunction of the Hamiltonian). Rather the true stationary states would be the orthogonal combinations of them, which can be written as,

$$\nu_1 = \cos\theta\ \nu_\mu - \sin\theta\ \nu_e \quad \text{and} \quad \nu_2 = \sin\theta\ \nu_\mu + \cos\ \theta\nu_e \tag{1.1}$$

Using simple calculations from quantum mechanics it can be shown that the probability of transforming ν_e to ν_μ is following

$$P_{\nu_e \to \nu_\mu} = \left[\sin(2\theta)\ \sin\left(\frac{E_2 - E_1}{2\hbar}t\right)\right]^2 \tag{1.2}$$

where t is time, $E_{1,2}$ are the energy of the stationary states $\nu_{1,2}$, and θ is called a mixing angle. This shows that the expression for probability is a sinusoidal function which means, ν_e will transform to ν_μ and ν_μ to ν_e back and forth analogous to oscillation from one state to another. Hence the name of the phenomena. For detailed discussion on neutrino oscillations, consult [3].

The NOvA experiment is primarily designed to investigate the oscillation from $\nu_\mu \to \nu_e$ by shooting ν_μ from Fermilab site and comparing the number of ν_e present at Fermilab site (near Illinois, Chicago) to the observed number of ν_e at a site near U.S - Canada border called Ash River, Minnesota, 810 km away from Fermilab. A secondary goal of the experiment is to greatly improve measurements of ν_μ disappearance parameters.

Components: The project consists of 3 main components, 1. a neutrino beam, 2. detector at Fermilab site called the Near Detector, and 3. detector at Ash River, Minnesota called the Far Detector.

1. **The NuMI Beam:** The **Neu**trinos at the **M**ain **I**njector (NuMI) neutrino beam was built at Fermilab to provide neutrinos for MINOS, a long-baseline neutrino oscillation search experiment which investigates disappearance of ν_μ as they travel through earth. However, this beam facility was later used for

other experiments like MINOS+, MINERvA, and NOvA. The NuMI beam is produced by 120 GeV protons hitting the 0.95 meter long graphite target which is essentially a Nucleon-Proton interaction that eventually produces a secondary beam of hadrons [5]. Two magnetic horns allow preferential selection of one or the other kind of charged hadrons. Pions and Kaons constitutes the major portion of the hadrons beam and predominantly decays to produce muons and neutrinos. Upon separating the muons from the decay products, the NuMI facility produces a nearly pure ν_μ beam. The reactions can be summarized as

$$N + P \rightarrow \pi^+ + K^+ \tag{1.3}$$

$$\pi^+ \rightarrow \mu^+ + \nu_\mu \tag{1.4}$$

$$K^+ \rightarrow \mu^+ + \nu_\mu \tag{1.5}$$

There is also a small anti muon-neutrino ($\bar{\nu_\mu}$) component coming from negative hadrons (π^-, K^-) and a small contamination of electron-neutrinos (ν_e) due to subdominant electronic decay mode of K^+ hadrons, decays of K^0 particles, and decays of tertiary muons.

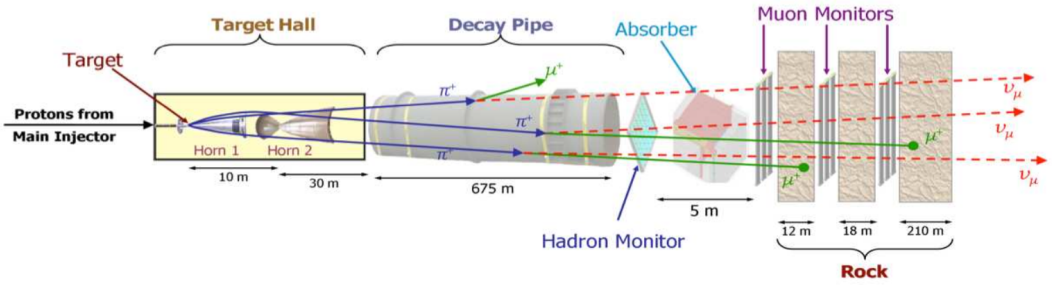

Figure 1.1: Schematic of the NuMI beam. All the important elements are shown together with relevant dimensions, including the target, the horns, the decay pipe, the hadron absorber, and the so-called muon shield which consists of the 240m long dolomite rock preceding the Near Detector. [5]

2. **The Near Detector:** As illustrated in Figure 1.2, the NOvA Near Detector (ND) is housed in an underground cavern off the existing MINOS access tunnel. This Near Detector location is 1002 meters away from the NuMI Target Hall and 105 meters below ground. As seen in Figure 1.3, the cavern and Near Detector

are placed off-axis at the same angle of 14.6 milliradians as the Far Detector in Ash River. Most parts of the Near Detector's design - PVC extrusions, modules, planes, blocks, and fiber readout were created for the Far Detector. They are utilized for the Near Detector as well to make it as comparable to the Far Detector as possible. The Near Detector size is $(3.9 \times 3.9 \times 12.8)m^3$ with mass 290 ton. Image of Near Detector is shown in the figure 1.5 alongside with the Far Detector image for comparison.

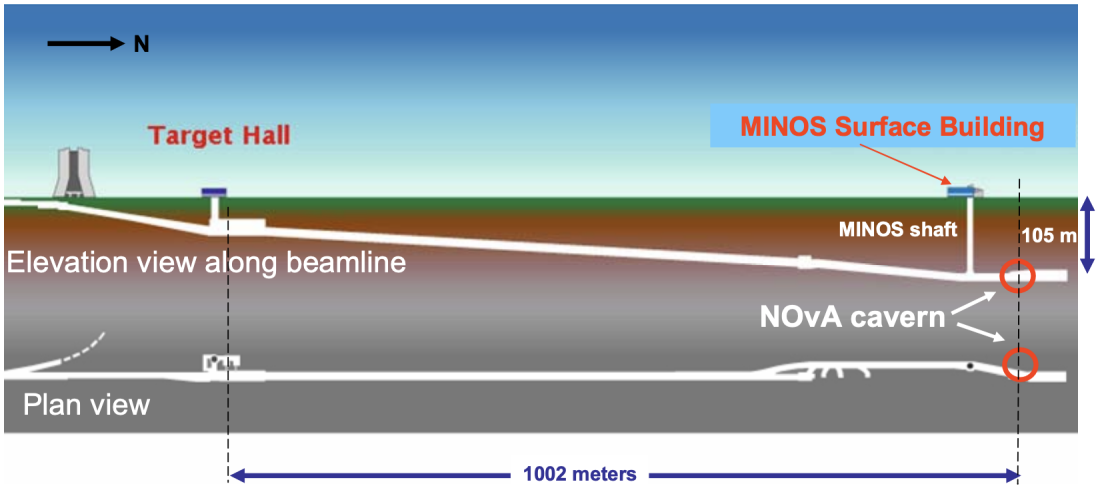

Figure 1.2: Plan and elevation view of the NuMI beam line. The NOvA Near Detector is located in the underground tunnel in the location labeled "NOvA cavern".[6]

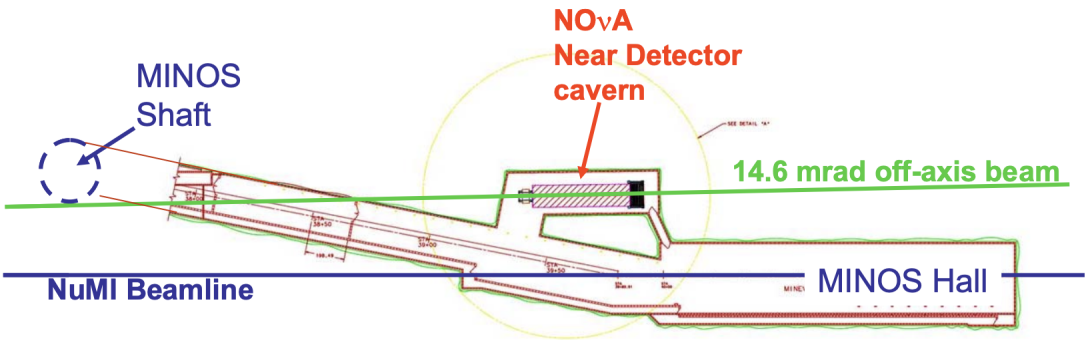

Figure 1.3: A detailed plan view of the MINOS access tunnel depicting that the Near Detector is off 14.6 milliradians from the NuMI beam axis.[6]

3. **Far Detector:** The NOvA Far Detector is located in the vicinity of Ash River, Minnesota, 810.5 kilometers away from Fermilab. The site is 11.8 kilometers west of the NuMI beamline, shown in figure 1.4. The dimension of the active detector is $(15.5 \times 15.5 \times 60)m^3$ with mass 14000 tons. A schematic diagram for both the Near and Far Detector is shown in figure 1.5.

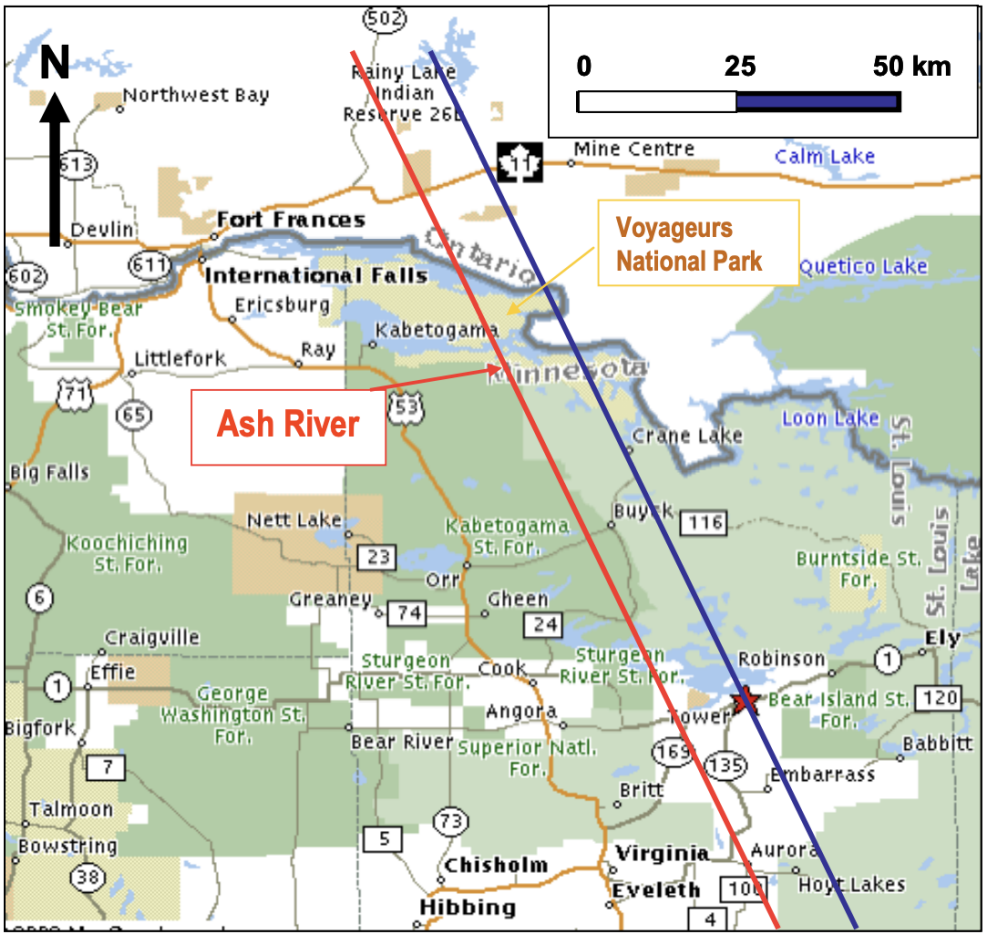

Figure 1.4: The Ash River Far Detector location is depicted on a map. The NuMI beam centerline (blue) passes past the MINOS detector (red star) underground at Soudan. The NOvA Ash River location is located 11.8 km (14.6 mradians) off-axis on the red line to the left (west) of the NuMI beam centerline. The location is located north of Voyageurs National Park and the US-Canada border. [6]

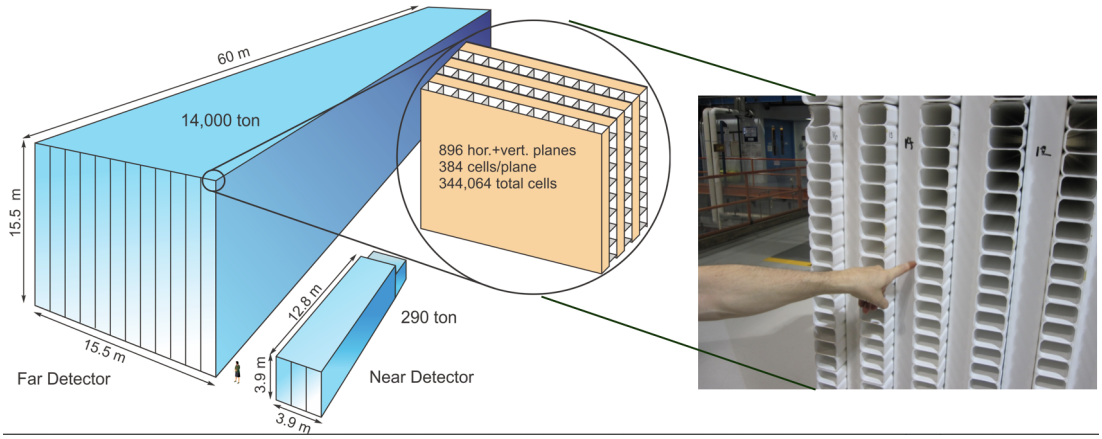

Figure 1.5: NOvA Near and Far Detectors shown with the dimension. The inset pictures shows the constituting part of the detectors. The detectors are made up off extruded PVC cell filled with liquid scintillator.[7]

Detector Elements:

- All NOvA Detectors are built around a simple rectangular rigid PVC plastic cell housing a liquid scintillator and a wavelength-shifting fiber. Charged particles travel mostly along the depth (D) of the cell and produce scintillator light. When charged particles interact with scintillator material, it deposits energy by exciting the scintillator atom. As these atoms comes to ground states from excited states, they release photons excess energy in the form of scintillator light. The light bounces about in the rectangular cell of width W, depth D, and length L until it is trapped by a wavelength-shifting fiber or absorbed by PVC or scintillator. At the top of the cell, both ends of the looping fiber are directed to one pixel on an Avalanche Photodiode (APD) photodetector array, and the light is converted to an electrical signal.

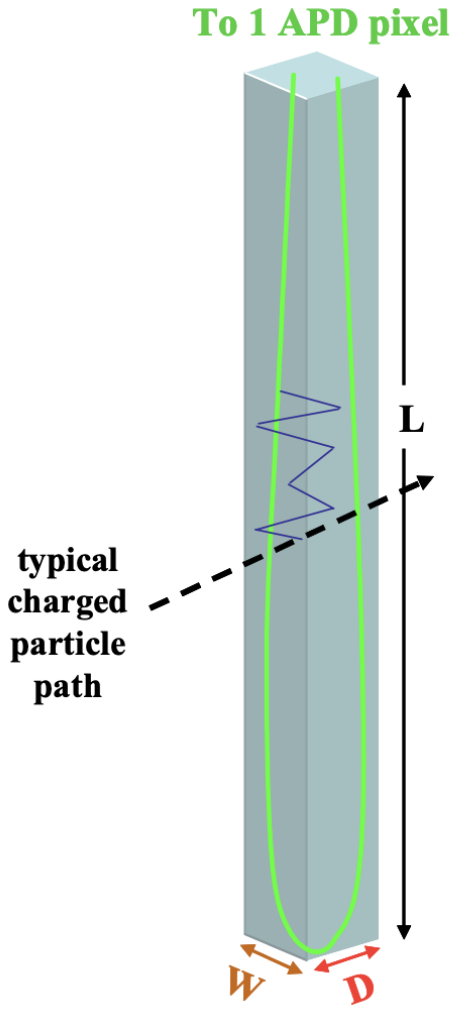

Figure 1.6: A PVC cell (W, D, L) with a liquid scintillator and a wavelength-shifting fiber (green). Light (blue line) is produced when a charged particle strikes the front face and bounces off the cell walls until it is absorbed by the fiber. The light is sent through the fiber to an APD.[6]

- The liquid scintillator stored inside the NOvA cells accounts for 70% (10.5 kilotons) of the NOvA detector mass. The 3.9 million gallons of liquid scintillator are mostly mineral oil with a scintillant of 4.1% pseudocumene [1,2,4-Trimethybenzene].
- The NOvA detector has around 13,000 kilometers of wavelength shifting fiber,

with each 15.6 m long cell carrying a 33.5-meter loop. The fiber absorbs blue light in the 400-450 nm region from the scintillator and changes the wavelength to green light in the 490-550 nm range.

For a detailed discussion on Detector elements, consult the NOvA Technical Design Report [6].

1.2 Motivation

In our experiment, it is essential to ensure accuracy and minimize noise to focus solely on neutrino interactions caused by the NuMI neutrinos inside the detectors. However, we encounter a significant amount of background interactions detected by both detectors consistently. Figure 1.7 illustrates a 5ms window of activity observed in the Far Detector.

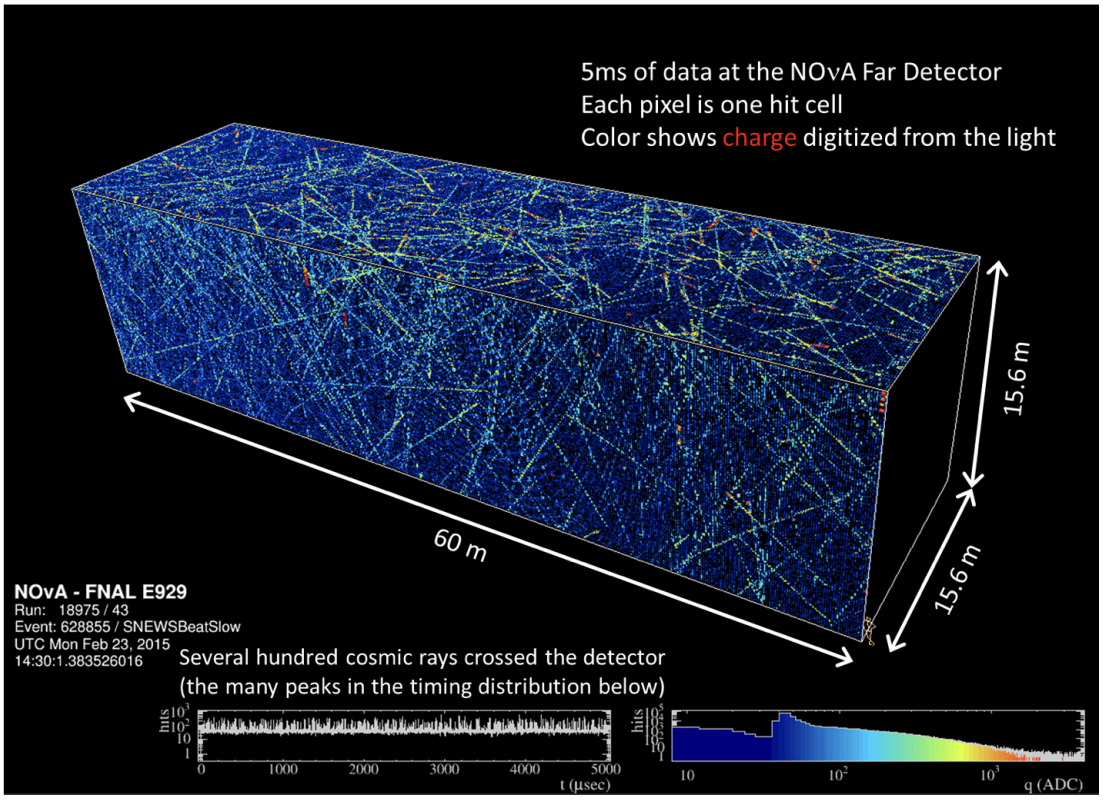

Figure 1.7: 5ms window of Far Detector data. Each pixel is one hit cell. [7]

The neutrino flux per unit mass in the Near Detector is approximately one million times higher than in the Far Detector. Consequently, the Near Detector exhibits considerably more activity. Additionally, our detectors are constantly bombarded by an extensive influx of cosmic muons. These muons are generated when cosmic rays interact with air molecules, and they approach our detectors from all directions. While we aim for an ideal situation with a pure neutrino beam from NuMI, the current muon catcher and rock region setup is insufficient to completely eliminate charged particles from the beam. Neutrinos produced from the decay of Pions and Kaons can interact with the rock nucleus as they traverse through the rock region, generating additional muons in the process.

$$\nu_\mu + N \rightarrow \mu^- + p \tag{1.6}$$

These are called *rock muons*. If this kind of interactions happen within few meter depths of rock region, the probability for the muon to penetrate the detector at the end of rock region is small, as it has to propagate a long distance of rock. However, when the interactions happen near the end of the rock region, there's a higher chance that these muons will be captured by the detector. This scenario is illustrated in Figure 1.8.

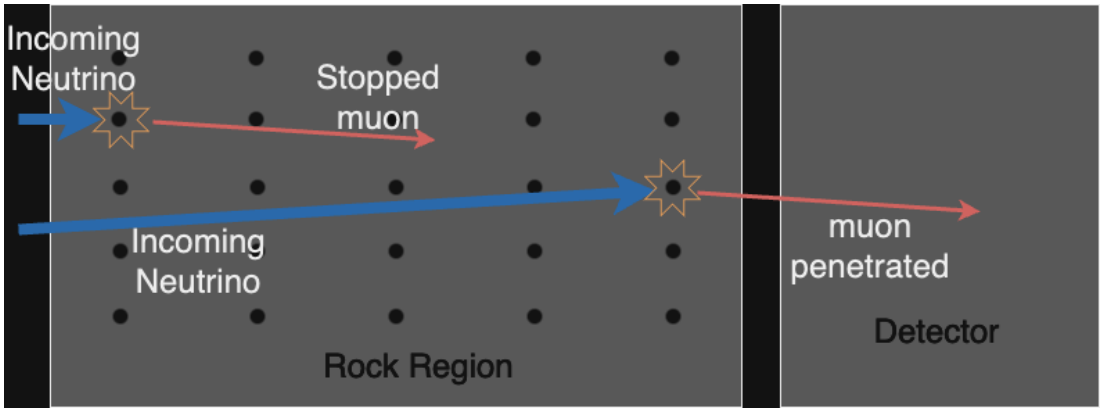

Figure 1.8: Incoming beam neutrinos interacting with rock nucleus and generates muons that can either get absorbed by the rock volume or penetrate detector region depending on its initial energy and origin point inside rock region.

To obtain an accurate description of the beam energy, it is crucial to understand how much of the beam energy is carried by muons before they reach the detector and while they are within the detector. To simulate the real experimental conditions, we

need precise modeling of the propagation of these muons through the vast volume of rock. Currently, NOvA is utilizing GEANT4 for this task, which is known for its accuracy but is computationally time-consuming due to its step-by-step working algorithm (as discussed in Chapters 3 and 5). The simulation of rock constitutes a significant portion, accounting for 52% of the total simulation time per batch [8]. This represents a substantial amount of time that could potentially be saved by using other simulation programs. Hence, we are motivated to explore the usage of PROPOSAL, a relatively new particle propagation tool that efficiently simulates lepton propagation through various media. For detailed information, please refer to Chapters 3 and 5.

Chapter 2

Charged Particle Interactions with Matter

Our study requires the understanding of particle propagation through medium in great detail. During their flight, particles come to interact with the constituent matter intensively. The interactions depends on the nature of the incident particle such as its mass, energy, momentum, direction as well as the mediums density, Z/A (Atomic number to weight) ratio, etc. Since we are dealing with muons, a charged particle, we will be discussing how charged particles interact with matter in this chapter.

Before we deep dive into the subject, it is important to disclose what we mean by the term "medium". A medium is the volume of matter through which the incident particle is propagating. Consider the case of Atmospheric Muons where the particles are being generated in the Earth's upper atmosphere and being detected in an underground detector. In this scenario, particles are moving through Air Medium (consisting mostly O_2 and N_2 molecules) and Earth Medium (consisting soil, rock, water, etc). Constituent matter of the medium influence the likelihood and characteristics of the interactions with incident particle. Consequently, the selection of "medium" in any particle physics experiment is a crucial subject.

In general, passage of charged particles through matter is characterized by three key processes,

1. **Elastic Interaction:** In elastic interactions, the total kinetic energy is conserved. In the context of elastic scattering, the potential energy is negligible or considered constant as the interaction forces or fields do not significantly change during the scattering process. The incident particle exchange energy and momentum with the target particle without altering either particle's identity. Elastic collisions between particles or elastic scattering of particles off atomic nuclei are two examples of elastic interactions.

2. **Inelastic Interaction:** In inelastic interactions, the incident particle gives the target particle energy and momentum, changing the target particle's identity or internal state. Excitations, ionizations, or particle generation are candidates of inelastic process. The system as a whole or the target particle may get excited as a result of the incident particle losing energy, resulting in further emissions of photons or particles. Excitation, Ionization, Bremsstrahlung, Pair (e^+e^-) Production, and nuclear reactions are examples of inelastic interactions.

3. **Multiple Scattering:** Multiple scattering is the result of several small-angle scatterings that a particle encounters while moving through a material. The Coulomb interactions between the charged incident particle and the charged particles in the medium cause these small-angle scatterings. The total distribution of particles in a detector or medium can be impacted by multiple scattering, which widens the particle's trajectory.

One of our main analysis tool PROPOSAL does not incorporate all these interactions in its current version. Therefore in the the subsequent sections, we will be discussing only the prominent mode of interactions that are integrated in PROPOSAL.

2.1 Ionization

For passage of particles though matter, one of the most common and prominent inelastic collisions mode is ionization. When a moderately relativistic charged particle propagates through a medium, it can transfer enough energy to knock off atomic electrons from their shells, resulting an ion and free electrons. This process is called as Ionization. The Feynman diagram in Figure 2.1 depicts the ionization process.

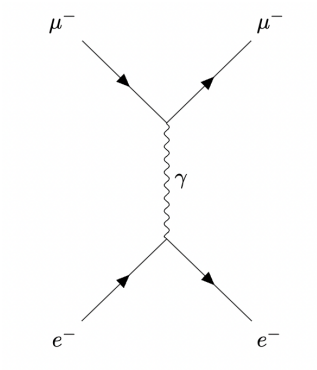

Figure 2.1: Feynman diagram for Ionization caused by incident muons. Incident muon comes to interact via electromagnetic force with the electron bound to atom and yields the final state of the electron free from the atom.

These collisions are of course statistical in nature occurring with certain probability predicted by quantum mechanics. However, it is possible to work effectively with the average energy loss (of the incident particle) per unit length due to the fact that the number of collisions per macroscopic path-length is large and their total energy loss fluctuates rarely. This quantity is called stopping power or dE/dx, which was first calculated by Bohr classically and later by Bethe, Bloch and others using Quantum Mechanics. Bohr's treatment parameterize the equation using impact parameter (b, which is not a measurable quantity) whereas the Bethe-Bloch equation is parameterized in terms of transferred momentum (a measurable quantity). The standard Bethe-Bloch equation is given in [9] as

$$-\frac{dE}{dx} = Kz^2\frac{Z}{A}\frac{1}{\beta^2}\left[\frac{1}{2}\ln\frac{2m_ec^2\beta^2\gamma^2T_{max}}{I^2} - \beta^2 - \frac{\delta}{2}\right] \tag{2.1}$$

where dx is thickness/length expressed in *mass thickness* unit.

$$mass\ thickness \equiv \rho.dx$$

where ρ is mass density and dx is thickness, which yields dimensions of mass per unit area, i.e., g/cm^{-2}. Other symbols are

- $K = 4\pi N_A r_e^2 m_e c^2$: a constant
- r_e, N_A: Classical electron radius, Avogadro's Number

- z, γ, β: charge of incoming particle, gamma factor, velocity $\beta = \frac{v}{c}$
- Z, A, ρ, I: charge and atomic number of medium atoms, density, average ionization potential for the medium.
- T_{max}, δ, m_e: Maximum Kinetic energy that can be imparted to a free electron in a single collision, density correction term, and electron mass.

The energy-momentum conservation principles set a limit on the amount of maximum energy an incoming particle may impart to an electron. For an incoming particle of mass M, velocity v, and gamma-factor γ:

$$T_{max} = \frac{2m_e\beta^2\gamma^2}{1 + 2\gamma\left(\frac{m_e}{M}\right) + \left(\frac{m_e}{M}\right)^2} \tag{2.2}$$

Key Points of Bethe-Bloch Formula:

- dE/dx depends on the charge of the incoming particle as z^2. Therefore for particle with greater value of charge, say, alpha particles, will lose more energy than, say, muon (assuming they both had same initial energy).
- A plot of dE/dx vs energy is shown below. At low energies, the $1/\beta^2$ term dominates dE/dx, which drops with increasing velocity until $0.96c$, at which point a minimum is obtained. Particles at this point are called *minimum ionizing particles (mip)*. For all particles with the same charge, the minimum of dE/dx is roughly the same. Beyond this point, $1/\beta^2$ remains almost constant (~ 1), but dE/dx steadily increases again owing to the logarithmic dependency of β^2 in $\ln \frac{2m_e c^2\beta^2\gamma^2 T_{max}}{I^2}$. This rise is cancelled however, by the density correction δ.

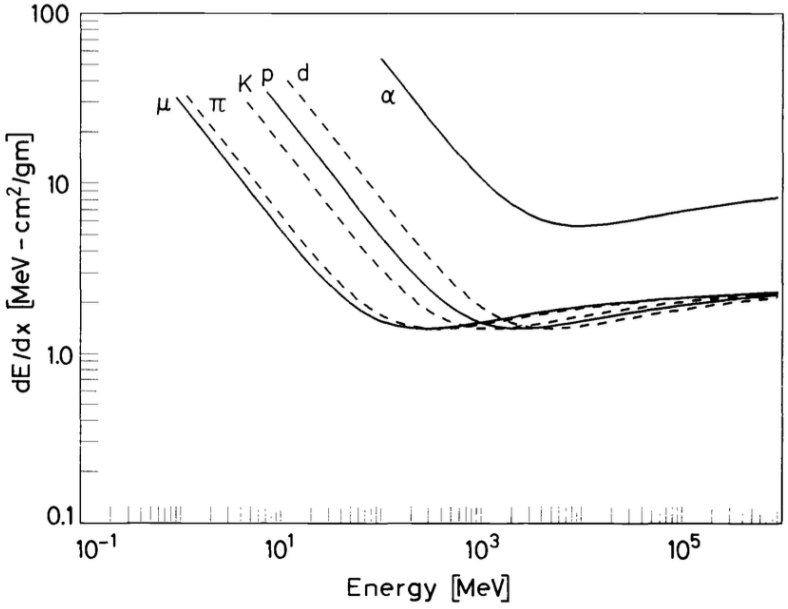

Figure 2.2: Stopping power dE/dx of muon (μ), pion (π), kaon (K), proton (p), d-meson (d), alpha particle (α) as a function of energy. [10]

Each particle has a unique dE/dx curve for energies below the *minimum ionizing* point. Physicists exploit this property frequently to identify particles in this energy range.

- Density Correction Term δ becomes significant at high energies. The original Bethe-Bloch formula makes the assumption that the medium is made up of separate, individual atoms. But this is not the case in practice. The effective charge that the incoming particle experiences can be decreased because the electron cloud of an atom can shield the electric field of far lying neighboring atoms. As a result, the particle's energy loss is a little less than what the original Bethe-Bloch formula predicts. This effect depends on the density of the material as the induced polarization by the incoming particle will increase with density.

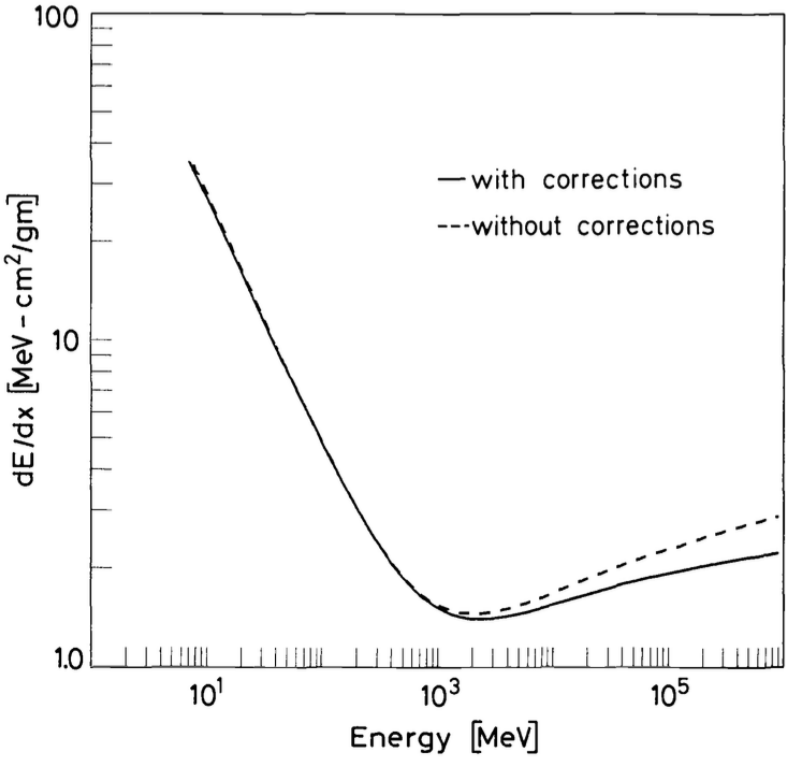

Figure 2.3: Comparison of the dE/dx vs energy of electron with and without the density correction consideration. [10]

- Dependence on Z/A ratio is crucial on the behavior of dE/dx since greater value of the former indicates higher chances of collision. Since Z/A ratio is atomic number relative to the atomic mass, a higher Z/A value implies greater density of atomic electrons, hence greater chances of interactions. However for most material Z/A is $\sim \frac{1}{2}$, which makes this a less important factor in the comparative analysis of Bethe-Bloch formula for those material. For NOvA rock region, the calculated $\frac{Z}{A}$ ration is $\frac{10.98}{11.32}$ [11].

- The impact parameter b corresponds to the perpendicular distance from the trajectory of the incident particle, defining the range within which it can exert influence on the surrounding atoms. This parameter is not directly measurable and its exact value depends on several factors, including the charge and momentum

of the particle, as well as the density of the medium and other contributing factors. While the Bethe-Bloch formula does not explicitly incorporate the impact parameter b, its influence is indirectly embedded through the mean excitation potential I and the maximum kinetic energy T_{max} as following.

$$I = 2\frac{z^2\alpha^2}{m_e v^2}\frac{1}{b_{max}^2} \tag{2.3}$$

$$T_{max} = 2\frac{z^2\alpha^2}{m_e v^2}\frac{1}{b_{min}^2} \tag{2.4}$$

where $\alpha = \frac{e^2}{2\epsilon_0 hc}$ is the structure constant. Since the measurement of both I and T_{max} is performed using other methods, this makes the Bethe-Bloch formula viable for experimental analysis.

- The most important parameter in the Bethe-Bloch formula is the **Mean Excitation Potential** I, which represents average amount of energy required to ionize an atom. It is a measurement of the ability of the medium to thwart the propagation of particles through it. Higher value of I signify that more energy is needed to ionize the atoms or excite their state, which causes the incident particle to lose energy more slowly. Theoretically, I can be understood from Bohr's atomic model. It is essentially the amount of energy required to free an electron from its shell, which is $h\bar{\nu}$, where h is Planck's constant and $\bar{\nu}$ is average orbital frequency. However, calculating this quantity in practice poses significant challenges due to the complex electron configurations of atoms, the presence of energy bands rather than distinct energy levels in solid materials, material heterogeneity, and other experimental factors. Therefore, values of I have been deduced empirically from measurements of dE/dx as a function of Z.

$$\frac{I}{Z} = 12 + \frac{7}{Z}eV; \text{ for } Z < 13 \tag{2.5}$$

$$\frac{I}{Z} = 9.76 + 58.8Z^{-1.19}eV; \text{ for } Z > 13 \tag{2.6}$$

A comprehensive list of I values can be found in the articles authored by Sternheimer et al. [12].

- The rate of energy loss increases as a particle slows down in matter because its kinetic energy decreases. At the end of its path, more energy will be deposited than at the beginning. This effect is seen in the following figure. This curve is known as the **Bragg Curve**. Initially, the particle loses minimal energy. However, as it moves deeper into the material, its energy loss increases until it reaches a peak value, known as the Bragg peak.

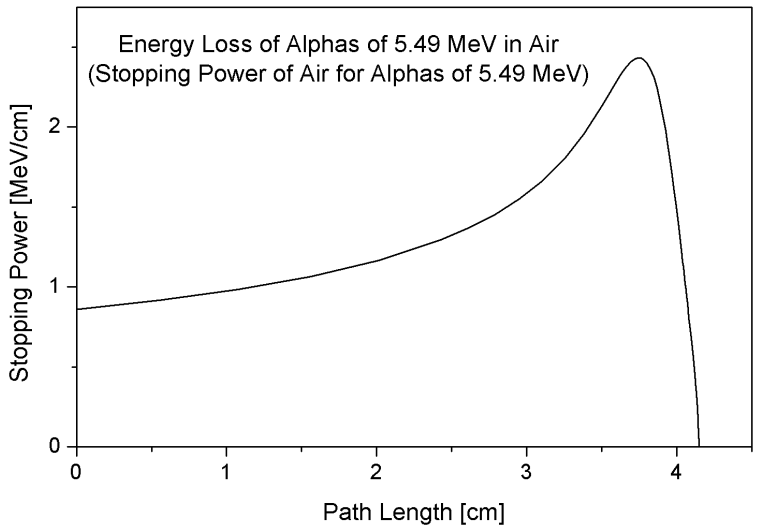

Figure 2.4: The Bragg curve showing the 5.49 MeV alpha particle energy deposition in air. This graph gives insight into the ionization behavior of alpha particles in the air medium by showing the distinctive peak where the energy deposition is highest. [13]

The energy deposition reaches its maximum when the particle's energy matches the optimal level for efficiently ionizing the atomic electrons, leading to the formation of a peak. After the Bragg peak, the particle begins to pick up electrons, which lowers the effective charge of the particle, resulting in a rapid decrease in dE/dx. Also, due to the decrease in electromagnetic interactions due to the particles lower momentum, the energy loss rapidly decreases. The position of the Bragg peak depends on the characteristics of the particle, as well as the characteristics of the material. The peak occurs at a specific depth, known as the

Bragg peak depth, which can be controlled by adjusting the energy of the particle or the choice of material. This behavior has medical applications for radiation treatment.

2.2 Bremsstrahlung

Relativistic charged particles, as they propagate through matter can undergo acceleration or deceleration due to the electric field of the surrounding atom resulting a change in trajectory from its initial path. This change will correspond to an emission of a photon. This is called Bremsstrahlung radiation. The name came from German which means braking radiation. The change in its momentum of the incoming particle can be thought of as a braking or slowing down effect, and hence the name. The cross section for this process depends on the particle mass as inverse square, $\sigma \propto r_e^2 = (e^2/mc^2)^2$; therefore in comparison to electron, radiation loss of this type by a muon is thus 40000 times smaller [10]. Since most sources and books provide the analysis taking into account electrons because radiation loss by electron is more significant than radiation loss by other charged particles, we will regard electrons as the incoming particles in this section for a general discussion of Bremsstrahlung.

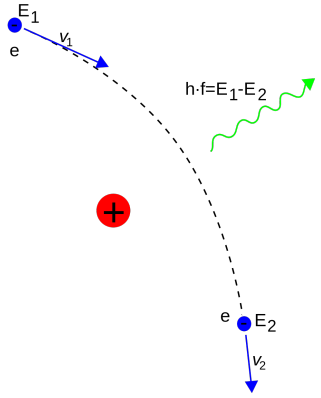

Figure 2.5: Bremsstrahlung process is illustrated, in which an electron with energy E_1 approaches the nucleus, loses energy as a photon of energy $h\nu$, and then passes with energy E_2. [14]

The degree of screening provided by the atomic electrons surrounding the nucleus is crucial because the intensity of the electric field that an electron experiences determines

how much Bremsstrahlung radiation occurs. This screening effect can be parameterized by:

$$\zeta = \frac{100 m_e c^2 h\nu}{E_0 E Z^{1/3}} \tag{2.7}$$

where, E_0 : Initial energy of the incoming particle; E : Final energy of incoming particle; $h\nu$: E_γ, Energy of emitted photon where ν is frequency from Plancks theory; Z : Atomic number of medium. ζ is related to the atomic radius and small ($\zeta \simeq 0$) for complete screening and large ($\zeta \gg 1$) for no screening.

For E_0 greater than a few MeV, Bremsstrahlung cross section can be found as following [15]:

$$d\sigma = 4Z^2 r_e^2 \alpha \frac{d\nu}{\nu} \left\{ (1+\epsilon^2) \left[\frac{\phi_1(\zeta)}{4} - \frac{1}{3} lnZ - f(Z) \right] - \frac{2}{3}\epsilon \left[\frac{\phi_2(\zeta)}{4} - \frac{1}{3} lnZ - f(Z) \right] \right\} \tag{2.8}$$

where, ϵ : $\frac{E}{E_0}$; α : Fine structure constant = $\frac{1}{137}$; $f(Z)$: Coulomb correction. It's a function that incorporates additional atomic effects; ϕ_1, ϕ_2 : Screening functions depending on ζ. Specific expression depends on considered model and approximations.

For heavy atom ($Z \geq 5$), ϕ_1 and ϕ_2 are calculated using the Thomas-Fermi atomic model [16] which agrees with empirical formula with an accuracy of 0.5% [17]

$$\phi_1(\zeta) = 20.863 - 2\ln[1 + (0.55846\zeta)^2] - 4[1 - 0.6\exp(-0.9\zeta) - 0.4\exp(-1.5\zeta)] \tag{2.9}$$

$$\phi_2(\zeta) = \phi_1(\zeta) - \frac{2}{3}(1 + 6.5\zeta + 6\zeta^2) \tag{2.10}$$

The function $f(Z)$ was calculated by *Davies* et al [18]. parameterized by $a = \frac{Z}{137}$ to be

$$f(Z) \simeq a^2[(1+a^2)^{-1} + 0.20206 - 0.0369a^2 + 0.0083a^4 - 0.002a^6] \tag{2.11}$$

For limiting cases of complete ($\zeta \simeq 0$) and no screening ($\zeta \gg 1$), it is easy to calculate the ϕ_1, ϕ_2 which ultimately equip us to calculate the Bremsstrahlung cross section 2.8. Thereafter energy loss can be calculated by integrating cross section times photon energy over the allowed energy range. ("rad" ≡ radiation)

$$-\left(\frac{dE}{dx}\right)_{rad} = N \int_0^{\nu_0} h\nu \frac{d\sigma}{d\nu}(E_0, \nu) d\nu \tag{2.12}$$

with N : number of atoms per volume ; ν : frequency of photon $= E_\gamma/h$. (To convince you, we can perform dimension analysis to 2.12. The left hand side is: $\frac{\text{Energy}}{\text{Length}}$. Right hand side is: $\frac{\text{Number}}{\text{Length}^3}(N) \times \text{Energy}(h\nu) \times \text{Length}^2(d\sigma)$, which yields the dimension of left hand side.) We can rewrite 2.12 as

$$-\left(\frac{dE}{dx}\right)_{rad} = NE_0\Phi_{rad} \tag{2.13}$$

where

$$\Phi_{rad} = \frac{1}{E_0}\int h\nu \frac{d\sigma}{d\nu}(E_0,\nu)d\nu \tag{2.14}$$

The reason behind this is, $d\sigma/d\nu$ is approximately proportional to ν^{-1} (with the proportionality constant depends on the medium specifics). Therefore, Φ_{rad} becomes independent of ν and becomes a function of material characteristics.

For $m_e c^2 \ll E_0 \ll 137 m_e c^2 Z^{-1/3}$, we have no screening ($\zeta \gg 1$), for which 2.14 yields,

$$\Phi_{rad} = 4Z^2 r_e^2 \alpha \left(\ln\frac{2E_0}{m_e c^2} - \frac{1}{3} - f(Z)\right) \tag{2.15}$$

and for $E_0 \gg 137 m_e c^2 Z^{-1/3}$, $\zeta \simeq 0$ (complete screening)

$$\Phi_{rad} = 4Z^2 r_e^2 \alpha \left(\ln(183Z^{-1/3}) + \frac{1}{18} - f(Z)\right) \tag{2.16}$$

At intermediate values of ζ, 2.12 must be integrated numerically.

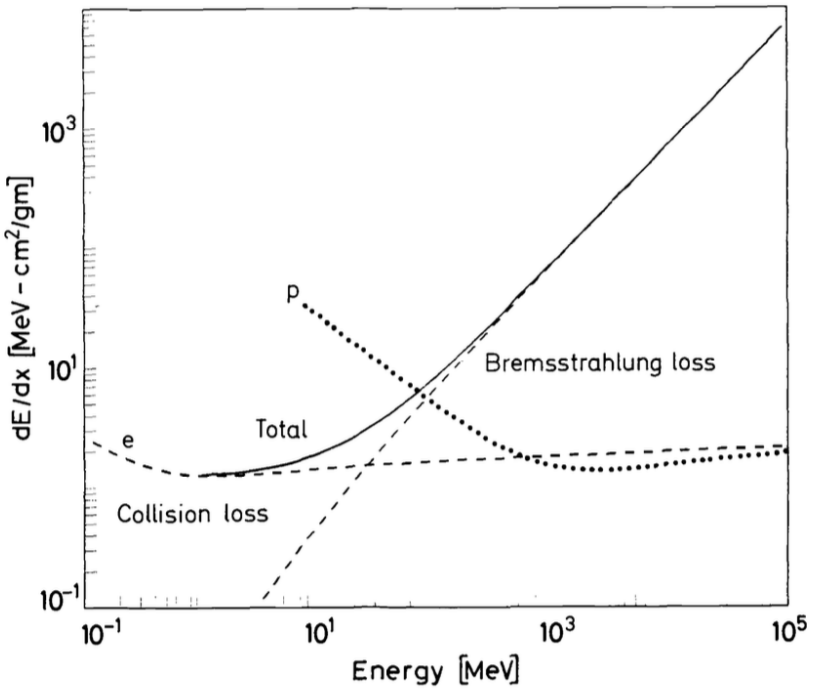

Figure 2.6: Comparison of energy loss for electrons in copper reveals the distinction between radiation loss and collision loss. The energy loss rate (dE/dx) for protons is also included for reference. [10]

Key Points of Bremsstrahlung Radiation:

- The ionization loss, given by 2.1, is logarithmically dependent on energies at high energy and linearly dependent on Z. One the other hand, Bremsstrahlung or radiation loss increases almost linearly with energy and quadratically with Z. [10]
- Unlike ionization, which is a quasicontinuous energy loss process, radiation energy loss can be emitted in one or two photons taking all the lost energy of the incoming particle. Therefore, a large energy fluctuation can be observed for mono energetic beam of particles.
- Radiation energy loss depends strongly on the medium material. For each material, it is useful to assign an energy value, defined as critical energy E_c of that

medium, at which radiation loss equals to the collision loss of ionization.

$$\left(\frac{dE}{dx}\right)_{rad} = \left(\frac{dE}{dx}\right)_{coll} \quad \text{for } E = E_c \tag{2.17}$$

Above this energy range, radiation loss will dominate over the ionization loss and vice-versa for below E_c. An approximate formula for E_c is given as:

$$E_c \simeq \frac{800MeV}{Z + 1.2} \tag{2.18}$$

The following table [10] gives a short list of E_c for different materials for incident electrons.

Material	Critical Energy E_C (MeV)
Pb	9.51
Al	51.0
Fe	27.4
Cu	24.8
Air (STP)	102
Lucite	100
Polystyrene	109
NaI	17.4
Anthracene	105
H_2O	92

- A quantity known as the *radiation length* is frequently used in energy loss by radiation analysis. It is the distance over which the incoming particle losses $1/e$-th of its initial energy. From 2.13,

$$-\frac{dE}{E} = N\Phi_{rad}dx \tag{2.19}$$

At high energies, Φ_{rad} is independent of E, therefore

$$E = E_0 \exp\left(\frac{-x}{L_{rad}}\right) \tag{2.20}$$

where, x is the distance travelled and $L_{rad} = \frac{1}{N\Phi_{rad}}$ is the radiation length. Using 2.14, L_{rad} can be found as

$$\frac{1}{L_{rad}} \simeq \left[4Z(Z+1)\frac{\rho N_a}{A}\right] r_e^2 \alpha[\ln(183Z^{-1/3}) - f(Z)] \tag{2.21}$$

A useful approximation is given in [9] as:

$$L_{rad} = \frac{716.4 g/cm^2 A}{Z(Z+1)\ln(287/\sqrt{Z})} \tag{2.22}$$

where, Z and A are the atomic number and weight of the medium material. Some values of L_{rad} is given for in following table.

Material	$[gm/cm^2]$	$[cm]$
Air	36.20	30050
H_2O	36.08	36.1
NaI	9.49	2.59
Polystyrene	43.80	42.9
Pb	6.37	0.56
Cu	12.86	1.43
Al	24.01	8.9
Fe	13.84	1.76

2.3 Pair Production

One of the important interactions for high energetic muons is when a fast muons interact with field of atomic nucleus to create a pair of electron and positron. When muon energy E_μ is at TeV range, the pair production cross section exceeds those of other muon interaction processes over a range of energy transfers between 100 MeV and $0.1E_\mu$ [19]. In TeV region, pair production accounts for more than half of the entire energy loss rate, with the average energy loss increasing linearly with muon energy. Following is the Feynman diagrams for two dominant mode of pair production interaction.

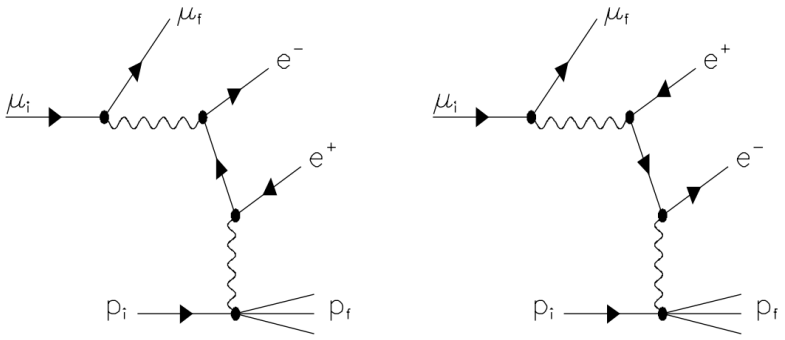

Figure 2.7: Feynman diagrams for the electron pair production in the field of an atom. $\mu_{i,f}$, $P_{i,f}$ are initial and final states for muon and target nucleus respectively. [20]

Key Points in Pair Production:

- This interaction is a dominant mode of energy loss in high energy. It is a stochastic energy loss process, therefore energy loss must be greater than the total rest mass of the produced pair particles in this interaction.
- The two dominant mode where incoming muons produce electron pair is shown in the relevant Fyenman diagram figure 2.7. These are called *electron mode* of pair production. However, *muon mode* and *tau mode can also happen*, but those sub-dominant mode of this interaction.
- The produced pair particles can cause further interaction with surrounding atom and lose energy through ionization, bremsstrahlung depending on its kinetic energy.

2.4 Photonuclear Interactions

The inelastic interaction of an atomic nucleus with a muon is described by the photonuclear interaction of muon where a virtual photon is exchanged between the incident and target particle. This is a dominant mode of interaction for muon at high energies ($E_\mu \geq 10$) GeV and at relative high energy transfer ($\nu/E_\mu \geq 10^{-2}$), where ν is the energy of secondary particle. It is crucial for the study of detector response to high energy muons, muon propagation, and muon-induced hadronic background, as well as for the study of light materials. The average energy loss increases almost linearly with

energy, and at TeV energy range of muons, this interaction constitutes 10% of the total energy loss rate. Following is the 1st order Feynman diagram for this process. [21]

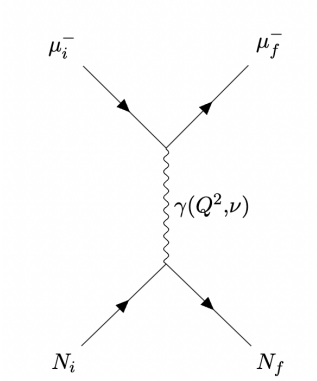

Figure 2.8: Feynman diagram for photonuclear interaction. $\mu_{i,f}^-$ and $N_{i,f}$ are initial and final state for incident muon and target nucleons respectively. Energy ν and four momentum transfer Q^2 are being mediated by the virtual photon.

Key Points in Photonuclear Interaction:

- Like Pair Production, Photonuclear Interaction is also a stochastic energy loss process. Meaning that the energy loss experienced by the muon during this interaction is not deterministic and cannot be precisely predicted for any individual event.
- The average energy loss in photonuclear interactions may increase almost linearly with the muon's energy, but the specific energy loss for individual interactions can vary stochastically.
- This process can cause the creation of protons, neutrons, pions, gammas as well as different kinds of hadrons depending on the incident energy and type of nucleus.

In one of our analysis "Secondaries Analysis", which is discussed in chapter 5, this interaction plays a vital role to generate many secondary particles for high incident energy. When we let a beam of muon pass through rock, We see a lot of secondary particles such as protons, neutrons and other hadrons are being produced, especially for $E_\mu \geq 10$ GeV.

Chapter 3

GEANT4

Simulation plays a fundamental role in an experimental physics project's design, evaluation and definition of the project's potential physics output, assessment of the experiment's performance, development, testing, optimization of reconstruction and physics analysis software, contribution to the calculation and validation of physics results and in many more domains. The GEANT4 object-oriented toolkit is a comprehensive collection of C++ libraries that enable the user to simulate their own detector system [1]. The software system autonomously transports the particles fired into the detector by specifying the detector shape and modeling particle interactions in matter using the Monte Carlo method which makes use of statistical sampling and random numbers to look for answers to mathematical problems.

GEANT4 is a free simulation toolbox which contains all facets of the simulation process, including [22]:

- the geometry of the system,
- the materials involved,
- the fundamental particles of interest,
- the generation of primary events,
- the tracking of particles through materials and electromagnetic fields,
- the physics processes governing particle interactions,

- the response of sensitive detector components,
- the generation of event data,
- the storage of events and tracks,
- the visualization of the detector and particle trajectories, and
- the capture and analysis of simulation data at different levels of detail and refinement.

User's own applications can be independent or built with the aid of another object-oriented framework. Geant4 will help them in both situations, from formulating the original problem through producing the data and graphics for publishing. For this purpose, the toolkit contains:

- user interfaces,
- built-in steering routines, and
- command interpreters

which operate at every level of the simulation.

The heart of Geant4 is an extensive collection of physics models to manage particle interactions with matter across a very broad energy range. It is developed in C++ and achieves transparency by utilizing advanced software engineering methods and object-oriented technologies. One of those spectacular features for example is, the way in which cross sections are input or computed is separated from the way in which they are used or accessed. The user can overload both of these features.

Similarly, depending on the energy range, the particle type, and the material, the calculation of the final state can be split into alternate or complimentary models. The user selects one of these options and inserts code into it's user action classes to create a particular application.

A major issue with earlier simulation programs was the difficulty of incorporating new or different physics models. Development was challenging because of the

procedure-based code's growing size, complexity, and interdependency. In contrast, object oriented methods manages complexity and limit interdependency by defining a uniform interface and common organizational principles for all physics models. Within this framework the functionality of models can be more easily identified and understood, and the creation and addition of new models is a well-defined procedure that entails little or no modification to the existing code.

3.1 History of GEANT4

The name "GEANT" stand for **GEometry ANd Tracking**. Also the word Geant came from the French word "géant", which means "giant" in English. The choice of this name reflects the large and ambitious nature of the Geant4 project, both in terms of the size and scope of the code and the international collaboration involved. The development of Geant4 began in 1993 with independent studies carried out at CERN and KEK to investigate the use of contemporary computer methods to improve the already-existing FORTRAN based Geant3 simulation tool. In 1994, these initiatives came together to produce a formal proposal to create a new software based on object-oriented technology. The project grew into a global partnership comprising physicists, programmers, and software engineers from numerous universities and institutes throughout the world. The initiative, which was initially centered on subatomic physics investigations, rapidly drew attention from other disciplines, including nuclear, accelerator, space, and medical physics. The partnership was renamed as Geant4 once the R&D phase was completed in 1998 and the first production release. In order to oversee the management, upkeep, user assistance, and continued development of the toolkit, a Memorandum of Understanding (MoU) was developed. Since then, Geant4 has developed into a massive undertaking, utilizing the knowledge of participants from many areas of Monte Carlo simulation. Its hierarchical structure and decentralized authority allow for effective user administration and assistance.

3.2 Overview of GEANT4 Functionality

The diagram for Geant4 class category is shown below:

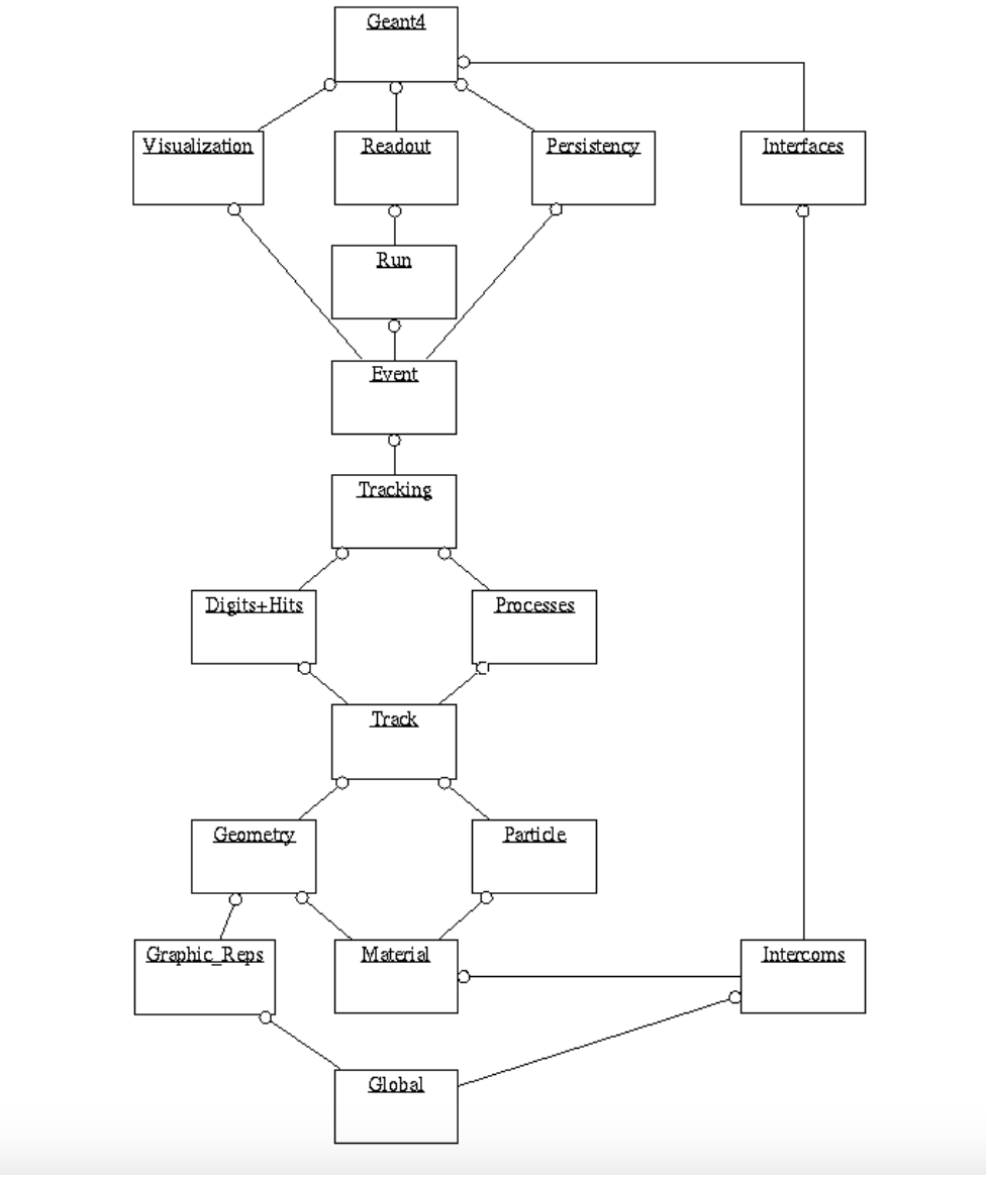

Figure 3.1: Geant4 Class Categories. Categories at the bottom of the diagram are used by virtually all higher categories and provide the foundation of the toolkit.

The

- **Global**

category covers the system of units, constants, numerical aspects and random number handling. Two categories

- **Materials**
- **Particles**

implement the tools required to characterize the material and particle characteristics needed to simulate particle-matter interactions.

- **Geometry**

describes a geometric structure and effectively transport particles across it using the module. The categories needed to explain particle tracking and the physical processes they go through are located above them. The

- **Track**

category includes classes for the tracks and stages that the

- **Processes**

category, in which the electromagnetic interactions of leptons, photons, hadrons and ions, as well as hadronic interactions, are implemented.
All processes are invoked by the

- **Tracking**

category, which controls their contribution to the evolution of a track's state and provides information in sensitive volumes for hits and digitization.
Above these, the

- **Event**

category manages events in terms of their tracks and the

- **Run**

category manages collections of events that share a common beam and detector implementation. And a

- **Readout**

category encompasses functionalities for simulating the response of detector elements to particles passing through them. It includes sensitive detectors to track energy depositions, hit collections to store relevant data, and digitization to mimic the detector's response, enabling accurate modeling of real-world experimental setups.

3.3 Units of Simulation

- **A Run:** As an analogy to the real experiment, a run of GEANT4 begins with "Beam On". Neither detector geometry nor physics process parameters may be changed during a run. This indicates that configuration of the simulation parameters for the detector is unavailable. A run is a collection of events that have the same detector circumstances [23].

- **An Event** At the start of processing, an event consists of primary particles, which are then placed into a stack. Processing continues until the stack is empty. The event is represented by the G4Event class, which holds the following objects after processing:

  - A list of primary vertices and particles.
  - Trajectory collection (optional).
  - Hits collections.
  - Digits collections (optional).

- **A Track:** A track in GEANT4 represents a snapshot of a particle, while a step provides 'delta' information to the track. The track is not a collection of steps, and it is removed under various conditions, such as

  - it goes out of the world volume,
  - it disappears (e.g. decay),
  - it goes down to zero kinetic energy and no "at rest" additional process is required,
  - the user decides to kill it.

  In Geant4, a track is composed of three layers of class objects: G4Track and G4DynamicParticle classes are unique for each track, while an object of G4ParticleDefinition is shared among all tracks of the same type.

- **A Step:** The step (class G4Step) is the fundamental unit of simulation; it comprises two points (pre-step and post-step). see Figure 3.2 . It carries incremental particle information (energy loss, elapsed time, and so on). Volume and material information are contained at each point. If the step is constrained by a boundary,

the end point stands exactly at the border but logically part of the next volume. As a result, boundary processes such as refraction and transition radiation can be simulated.

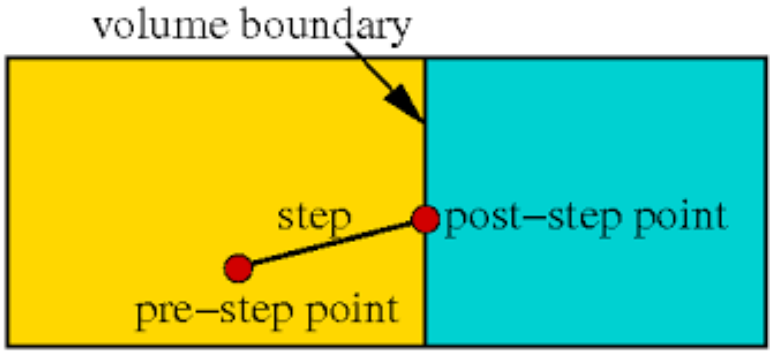

Figure 3.2: Step in Geant4. Here, color coded regions defines distinct volume. If the step is constrained by a boundary, the end point stands exactly at the border but logically part of the next volume. [24]

In our GEANT4 code, we exploited this "step" feature to collect data at some particular distance to calculate scattering angle during the flight of the particles. The step feature can be accessed by using TrajectoryPoints method in GEANT4 where $i+1$ refers to the post-step point if i refers to the pre-step point. For example, we asked for each particle, **if** the "TrajectoryPoint(i+1)s distance from starting position" is greater than 500 cm, **and** "TrajectoryPoint(i)s distance from starting position" is less than 500 cm, **store** the particle state information (to calculate scattering angle of the particles at propagation distance 500 cm).

Chapter 4

PROPOSAL

PROPOSAL (**PRopagator with Optimal Precision and Optimal Speed for All Leptons**) is a powerful Monte Carlo simulation library written in C++ with convenient Python bindings. Developed with the aim of providing both high performance and accurate simulations, PROPOSAL specializes in modeling the behavior of high-energy muons over long distances within different media. This capability is particularly crucial for large volume detectors like neutrino telescopes and subsurface experiments, as they often encounter a significant atmospheric muon background.

The versatility of PROPOSAL is demonstrated by its current usage in various scientific endeavors. It is extensively employed in the simulation chains of IceCube, ANTARES and RNO (Radio Neutrino Observatory), where it accurately simulates muon propagation and decay as well as the behavior of Taus (heavy leptons). It is used in the CORSIKA 8 air shower simulation software, specifically in calculating the electromagnetic component. This component encompasses the propagation of electrons, positrons, and high-energy photons, offering valuable insights into the development and characteristics of extensive air showers.

The robust combination of precision and efficiency provided by PROPOSAL makes it an indispensable tool for researchers and scientists in the field of particle and astroparticle physics. Its accurate simulations enable the optimization of detector designs, the analysis of lepton signals amidst background radiation, and the investigation of lepton transport phenomena in a variety of experimental and astrophysical contexts.

Moreover, the integration of PROPOSAL within simulation frameworks enhances the understanding of cosmic ray showers, aids in modeling astrophysical sources, and assists in studying phenomena like gamma-ray bursts and supernovae.

4.1 Energy Loss Calculation

The basis of particle propagation in PROPOSAL is the energy losses of particles. Assuming a particle with initial energy E_i, energy loss is described by an absolute value

$$\nu = E_i.v \tag{4.1}$$

where v describes the relative energy loss of the particle. Final energy of the particle is then, $E_f = E_i - \nu$. The implemented processes causing energy losses are

- Ionization
- Bremsstrahlung
- electron-positron Pair Production
- Photonuclear Interaction (as discussed in Chapter 2)

Quantitatively, the cross section σ is the interaction probability for a process. To describe the interaction probability with respect to a specific variable in the final state, for example lost energy ν, the cross section can be written in a differential form $d\sigma/d\nu$.

In principle, this information could be utilised right away to sample energy losses from differential cross sections, which are treated as probability density functions, by using inverse sampling. A probability distribution function (PDF) is a mathematical function that explains the probability distribution of a random variable. In this case, the differential cross section acts as a PDF for the individual variable of interest, i.e. ν in the interaction's final state.

$d\sigma/d\nu$ can be thought of representing the probability of interaction per unit of the variable ν. It describes how the probability of the interaction changes as a function of ν. By integrating the differential cross section over a specific range of ν, we can obtain

the total probability of the interaction occurring within that range.

To treat differential cross section as PDF, it must satisfy certain properties. First, it must be non-negative, meaning that the probability for a given value of ν cannot be negative. Second, the total probability over all possible values of ν must be unity.

By normalizing the $d\sigma/d\nu$ appropriately, it can be transformed into a PDF. This normalization involves dividing the differential cross section by the total cross section, integrating it over all possible values of ν, and then multiplying it by a normalization constant to ensure that the integral equals unity.

Once $d\sigma/d\nu$ is treated as a PDF, techniques such as inverse sampling can be employed to generate random values that follow the observed distribution. These sampled values can then be utilised to simulate the behavior of the particles during the interaction. The process can be summarized as following

1. Assume we have a differential cross section $d\sigma/d\nu$ as a function of ν. The probability per unit of ν is represented by this differential cross section.

2. First, we must integrate the differential cross section to produce the cumulative distribution function (CDF), which reflects the accumulated probability up to a certain ν value. Let's denote that CDF $F(\nu)$.

3. The inverse of the CDF is then calculated, denoted as $F^{-1}(p)$, where p is a uniformly distributed random number between 0 to 1.

4. Then we pass a uniformly distributed random number p through the inverse of the CDF, obtaining $\nu = F^{-1}(p)$. This value of ν will follow the distribution defined by the differential cross section.

Problem: However, this approach poses two immediate problems.

1. The propagation process would be extremely time-consuming due to small energy losses, especially below the energy threshold of a detector, and would be sampled individually

2. Numerical issues will arise, due to the nature of bremsstrahlung interaction: since photons are massless, bremsstrahlung cross section diverges for $\nu \to 0$; inverse sampling throughout the whole parameter range is thus impossible.

Solution: PROPOSAL differentiates between continuous and stochastic losses. The energy cut parameter is defined as

$$\nu'_{cut} = min[e_{cut}/E, \nu_{cut}] \tag{4.2}$$

with a relative energy cut ν_{cut} and an absolute energy cut e_{cut}. Energy losses with $\nu > \nu'_{cut}$ are considered stochastic losses, which means that each interaction with a relative energy loss above the cut is addressed individually. However, energy losses with $\nu < \nu'_{cut}$ are handled as continuous losses, which means that an averaged energy loss per distance is derived from all energy losses below the cut and applied to particles during propagation. Both e_{cut} and ν_{cut} parameters can be adjusted or deactivated separately. The specification in 4.2 assures that losses beyond an absolute detector threshold e_{cut} are recognized as stochastic even if their relative value is less than ν_{cut} by activating both parameters at the same time.

PROPOSAL's propagation algorithm consists of several, consecutively executed steps, each of which consists of continuous losses and stochastic loss. To perform one propagation step, it is necessary to have a mathematical expression to sample the next stochastic loss. Let, E_i be the initial energy of a particle and

$$P(E_f \leq E \leq E_i) = -\int_{E_i}^{E_f} p(E)dE \tag{4.3}$$

is a cumulative distribution function describing the probability for a stochastic loss at a particle energy $E \geq E_f$ [25]. This function can be used to find the E_f by utilising inverse sampling method. But first we need to have a formula for $P(E)$. Let the distance between the initial particle position x_i and the position of stochastic loss x_f is discretized into several Δx sections. Then the probability for a stochastic loss after a distance of $x_f - x_1$, without any stochastic losses in the interval (x_i, x_f), can be described as

$$\begin{aligned}\Delta P(x_f) &= P(x_f + \Delta x) - P(x_f) \\ &= (1 - \sigma(x_i)\Delta x_i) \cdot (1 - \sigma(x_{i+1})\Delta x_{i+1}) \cdot \ldots \cdot (1 - \sigma(x_{f-1})\Delta x_{f-1}) \cdot \sigma(x_f)\Delta x_f \\ &\approx \exp\left(-\sum_{j=i}^{f-1} \sigma(x_j)\Delta x_j\right) \cdot \sigma(x_f)\Delta x_f \end{aligned} \tag{4.4}$$

Each factor $(1 - \sigma(x_i)\Delta x_i)$ represents the complementary probability of not having an interaction at the specific value of x_i, multiplied by the small increment Δx_i. Here, $\sigma(x_i)$ represents the interaction probability (cross section) at the particular value x_i. Terms from $j = i$ to $j = f-1$ are approximated to exponential multiplied by $\sigma(x_f)\Delta x_f$ where stochastic loss occur. In differential form, this can be written as

$$dP(x_f) = \exp\left(-\int_{x_i}^{x_f} \sigma(x)\, dx\right) \cdot \sigma(x_f)\, dx_f \tag{4.5}$$

To convert the dependency on location x to a dependency on energy E, the relation

$$f(E) = -\frac{dE}{dx} = E\frac{N_A}{A}\int_{\nu_{min}}^{\nu'_{cut}} \nu \frac{d\sigma}{d\nu} d\nu, \tag{4.6}$$

with the Avogadro number N_A and the mass number A of the current medium, is introduced. Here $f(E)$ is the continuous energy losses between two stochastic losses and is derived by averaging the energy losses for all interactions below the energy cut ν'_{cut}. Applying 4.6 in 4.5 yields

$$dP(E_f) = \exp\left(\int_{E_i}^{E_f} \frac{\sigma(E)}{f(E)}\, dE\right) \cdot \frac{\sigma(E_f)}{-f(E_f)}\, dE_f. \tag{4.7}$$

Now, the $P(E)$ can be found by integrating over the probabilities in 4.7

$$\begin{aligned} P(E_f \leq E \leq E_i) &= \int_{P(E_i)=0}^{P(E_f)} dP(E_f) \\ &= \int_{E_i}^{E_f} \exp\left(\int_{E_i}^{E'_f} \frac{\sigma(E'_f)}{f(E)}\, dE\right) \cdot \frac{\sigma(E'_f)}{-f(E'_f)}\, dE'_f. \end{aligned} \tag{4.8}$$

Above expression can be simplified by considering

$$u(E) = \int_{E_i}^{E_f} \frac{\sigma(E')}{f(E')}\, dE', \qquad du = \frac{\sigma(E)}{f(E)}\, dE \tag{4.9}$$

Therefore, $P(E)$ becomes

$$\begin{aligned} P(E_f \leq E \leq E_i) &= -\int_{E_i}^{E_f} \exp(u(E'_f))\, du \\ &= \left[\exp(u(E'_f))\right]_{E_f}^{E_i} \\ &= \exp(u(E_f)) - \exp(u(E_i)) \qquad \text{but,} \quad \exp(u(E_i)) = 0 \\ &= \exp\left(\int_{E_i}^{E_f} \frac{\sigma(E_i)}{f(E)}\, dE\right) \end{aligned} \tag{4.10}$$

By equating $P(E)$ in 4.10 to a random number $\xi \in (0, 1]$, the energy integral

$$\int_{E_i}^{E_f} \frac{\sigma(E)}{-f(E)}\, dE = -\log \xi \tag{4.11}$$

is obtained. By sampling ξ, 4.11 can be used to calculate the final energy E_f.

4.2 Propagation Algorithm

PROPOSAL's propagation algorithm simulates the properties of secondary particles created in the interactions as well as the properties of primary particle after each interactions. This includes data on the energy, position, direction, and timing of the primary and secondary both particles.

The structure of the propagation process in PROPOSAL is dictated by the idea of a "chain of responsibility". The **Sector** objects and a **Propagator** object are the key components of this chain.

Each Sector is characterized by its geometry, which describes the spatial extent of the Sector. It also includes information about the medium present within the Sector, such as its composition and density, energy cut settings. The cut settings itself distinguish between distinct particle locations relative to a preset Detector, which is an area with higher propagation accuracy. By defining Sectors with varying characteristics, users have the flexibility to appropriately model the simulation environment.

The Propagator object determines which Sector is in charge of the particle's propagation at its current location. The assigned Sector then propagates the particle,

within its borders and returns the particle to the Propagator object. This procedure is continued until either the original particle's propagated distance exceeds a preset maximal propagation distance d_{max} or the initial particle's energy falls below a predefined threshold energy e_{low}.

Following steps give simplified view of propagation within a sector.

4.2.1 Energy of The Next Interaction

The remaining particle energy E_f just before the next stochastic loss is sampled using a random number ξ, according to equation 4.11. If

$$\xi > \exp\left(\int_{E_i}^{e_{low}} \frac{\sigma(E)}{f(E)}\, dE\right), \tag{4.12}$$

then the sampled energy E_f would fall below the threshold energy e_{low}. In this case, there is now stochastic energy loss.

On the other hand, if the propagated particle is capable of decaying, an energy value E_τ is sampled for the decay based on the particle's lifetime τ. Both the sampled energy values, E_f and E_τ, are compared, and the higher energy value, along with its associated interaction type (stochastic loss or decay), is selected for the next step in the propagation process.

4.2.2 Particle Displacement and Elapased Time

Given the initial energy E_i and the energy of the interaction E_f, the straight-lined displacement is calculated with the tracking integral

$$x_f = x_i - \int_{E_i}^{E_f} \frac{dE}{f(E)} \tag{4.13}$$

where $x_f - x_i$ is the propagated distance. If the calculated propagated distance of the particle is such that it would exceed the distance to the sector border d, a recalculation of the remaining particle energy, E_f, is required. Recalculation is done be setting $x_f = x_i + d$ in 4.13 and solving the integral equation for E_f. No interaction will occur at E_f in this case.

Calculation for elapsed time is straightforward using time integral

$$t_f = t_i + \int_{x_i}^{x_f} \frac{dx}{\nu(x)} = t_i - \int_{E_i}^{E_f} \frac{dE}{f(E)\nu(E)} \tag{4.14}$$

where ν is particle velocity. Alternatively, the approximation $\nu = c$ can be used to get

$$t_f \approx t_i + \frac{x_f - x_i}{c} \tag{4.15}$$

Chapter 5

Results

5.1 Why PROPOSAL is Faster Than GEANT4

PROPOSAL and GEANT4 are both Monte Carlo simulation tools for studying the passage of particles through matter. However, their method of operation is different which ultimately yields one of them more accurate but computationally expensive and the other faster but less precise.

PROPOSAL is designed specifically for the study of lepton propagation, while GEANT4 is a more general-purpose tool that can be used to simulate the passage of a wide variety of particles through matter. PROPOSAL uses up-to-date cross sections for lepton interactions, while GEANT4 uses a variety of cross sections that may or may not be up-to-date. PROPOSAL is designed to be fast and accurate, while GEANT4 is designed to be flexible and extensible.

The basic principle of a Monte Carlo based propagation tool like GEANT4 can be understood as following steps:

1. **Geometry definition, particle generation and initialization:** Define the geometry of the material the particle will propagate through. This involves specifying volumes, materials, and their properties (e.g., density, atomic composition).Generate particles with their initial properties, such as energy, position, direction, and type (electron, muon, etc.). Set up the event loop for multiple particles or events.

2. **Event Loop:** Start the simulation event loop to propagate particles through matter.

3. **Particle Tracking:** For each event, initialize the particle's position and direction based on the initial properties.

4. **Step-by-step Propagation:**

    - **A random number is generated:** Use a random number generator to produce a random value between 0 and 1.
    - **Interaction Selection:** Based on the random number and physics models, select the type of interaction that occurs during the current step. This could include scattering, energy loss (ionization, Bremsstrahlung), decay, particle creation, or other processes.
    - **Interaction Process:** Implement the specific interaction process corresponding to the selected type. Update the particle's properties, such as momentum, energy, and direction, according to the outcome of the interaction.
    - **Repeat:** Repeat the previous steps until the particle leaves the material or interacts with another particle:

5. **Multiple Particle Handling:** If the event loop involves multiple particles, propagate each particle independently in similar fashion, considering their respective properties and interactions.

6. **Importance Sampling (Optional):** If necessary, use importance sampling techniques to bias the random number generation and focus on rare events or interactions.

7. **End of Event Loop:** After completing all events, analyze the accumulated data to obtain statistical distributions and final simulation results.

However, PROPOSAL differs from the step-by-step method of Monte Carlo particle propagation in several ways which allows it to be faster and more efficient for simulating high energy leptons [25].

1. **Continuous Energy Loss:**

- In GEANT4, the Monte Carlo method is commonly employed to simulate continuous energy loss processes like ionization and Bremsstrahlung. However, this simulation technique breaks down these processes into small discrete steps. This approach can be computationally demanding, particularly for high-energy particles that undergo numerous interactions. As these interactions create multiple secondary particles, each requiring the same step-by-step treatment, simulation time grows exponentially, leading to increased computational costs.
- PROPOSAL, on the other hand, uses continuous energy loss models based on parameterizations and approximations, avoiding the need for a detailed step-by-step simulation.
  - PROPOSAL calculates the energy loss parametrizations through numerical integrations of the energy loss distribution (see equation 4.11). These integrations consider the characteristics of the particle and the material it is traversing through.
  - The results of these integrations are stored in interpolation tables, which provide a faster and more efficient way to access the energy loss values at different energies.
  - When propagating the particle, PROPOSAL uses random number generation to sample the energy loss from the interpolation tables. Importance sampling techniques may be employed to focus on regions of the energy loss distribution that contribute significantly to the overall energy loss.

  Since the same numerical integration is performed for all energy range, these simplification makes it computationally faster for high-energy leptons.

2. **Stochastic Energy Loss Fluctuations:**

- In the step-by-step approach, the energy loss of particles is sampled stochastically at each step, which leads to fluctuations in the energy loss and requires a significant number of steps for accuracy.
- PROPOSAL uses stochastic energy loss fluctuations efficiently through parametrizations and statistical methods, energy-cut settings, resulting in faster simulations while still capturing the essential energy loss distribution.

3. **Energy Loss Pre-Tabulation:**

    - PROPOSAL pre-tabulates energy loss and other relevant parameters to efficiently look up the required information during the simulation, reducing the computational overburden.
    - GEANT4, being a general-purpose toolkit, do not have pre-tabulated data for specific particle types or scenarios, making it less optimized for certain applications like high-energy lepton propagation.

Though it performs numerical integration to calculate energy loss, PROPOSAL is still considered as a Monte Carlo based propagation tool, because

1. **Random Number Generation :** PROPOSAL, like other Monte Carlo simulations, utilize random numbers to sample from probability distributions and make probabilistic decisions during the particle propagation. For example, when simulating energy loss processes or scattering angles, random numbers are generated to determine the sample from those energy loss or scattering distributions.
2. **Stochastic Energy Loss :** Although PROPOSAL uses parameterizations and approximations for continuous energy loss processes, it still incorporates stochastic fluctuations in energy loss. This is crucial to capturing the statistical nature of particle interactions.
3. **Probabilistic Interaction Selection :** PROPOSAL probabilistically selects various interaction processes based on their cross-sections and interaction probabilities, similar to the standard Monte Carlo method.

Figure 5.1 presents my result of running same experiment on GEANT4 and PROPOSAL. The plot shows real time taken for simulating 3000 muons of 3, 7, 10 and 40 GeV to pass through NOvA rock.

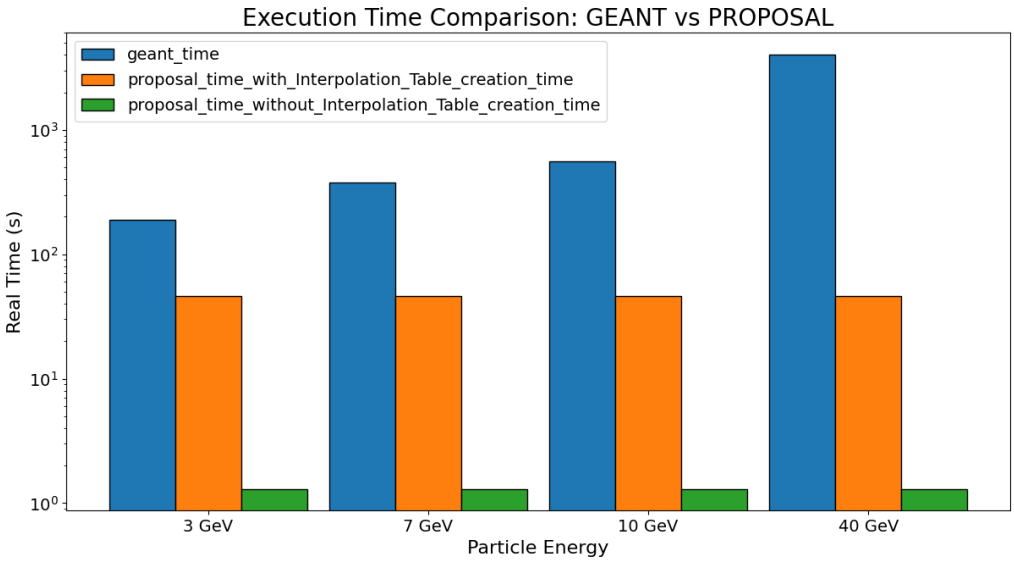

Figure 5.1: Real execution time comparison between GEANT4 and PROPOSAL for 3, 7, 10, 40 GeV muon passing through NOvA rock. Y axis is shown in log scale. Blue Bar represents GEANT4 time, Orange and Green bar represents PROPOSAL time considering and not considering time required to create interpolation table, respectively.

The blue bar represents the GEANT4 time and the orange and green bar represents PROPOSAL time "with" and "without" the time required to create interpolation table respectively. It means that, when a PROPOSAL code run for the first time, it takes almost a minute (depending on the desired accuracy) to set up the simulation. After the interpolation table is created, every later run is performed in less than 10 seconds. However, these values of PROPOSAL time of course depends on the specific values of energy cut settings. For our current concern for NOvA rock, I found out that the relative energy cut value of 0.0148 in PROPOSAL makes the best agreement with GEANT4 results. From the plot we see that, execution time for GEANT4 is almost 2 order of magnitude longer for low energy case like 3 GeV and more than 3 order of magnitude longer for high energy case like 40 GeV in comparison to PROPOSAL time without the interpolation table.

5.2 Comparison Between GEANT4 and PROPOSAL

The main focus of my thesis was to compare between GEANT4 and PROPOSAL for NOvA rock region. The near detector (ND) in NOvA is situated underground of ≈109 m of rock and soil. This is called "Rock Overburden" region. Also downstream to the NuMI beam, there's a rock region of ≈240m, which shield the various kinds of hadrons and charged particles. Since PROPOSAL is fast in execution and flexible for implementing geometries, simulating particles through dense medium like rock can help us to save NOvA simulation time. For that, we first need to validate whether the behaviour of simulation by PROPOSAL is similar enough to the current simulation tool GEANT4. To this extent, I ran experiment on both GEANT4 and PROPOSAL, ensuring same initial conditions and geometries, to investigate the nature of 2 characteristics features.

1. **Propagated distance:** PROPOSAL offers the value of propagated distance of each particle in its built-in function in "particle state" class. For GEANT4 experiment, I calculated propagated distance using Pythagoras law on initial and final state coordinate values.

2. **Scattering angle in position space**: I am calculating only Y axis scattering

$$\text{scattering angle} = \cos^{-1} \frac{\text{Difference between initial and final state Y coordinate}}{\text{Propagated distance}} \tag{5.1}$$

   The initial motion of the particles is along negative Y axis.

By "position space", I simply meant the angle between the initial state position vector and final state position vector. We can conceptualize similar kind of angle between initial state and final state momentum vector. That would be called as scattering angle in momentum space.

5.2.1 Experiment Setup

Particle type: muons
Number of particles: 3000.
Energies: {3,7,10,40} GeV
Particle motion: Along negative Y axis, i.e. from the earth surface to Near Detector.

Medium and density: Rock composition with $\frac{Z}{A}$ ratio being $\frac{10.98}{22.32}$. Density 2.41 gm/cc.

Figure 5.2 and 5.3 represents a schematic diagram for respective code environment for GEANT4 and PROPOSAL in this analysis. The only difference between two picture is that, in PROPOSAL, I defined a geometry, "Test Volume", submerged inside the rock geometry 500cm away from the earth surface, with volume 1000^3 cc, with center at (0,9000,500). For GEANT4, I simply considered imaginary lines for the "Test Volume" boundaries along Y axis. The usage of this "Test Volume" is to compute the scattering angle in mid flight of the particles.

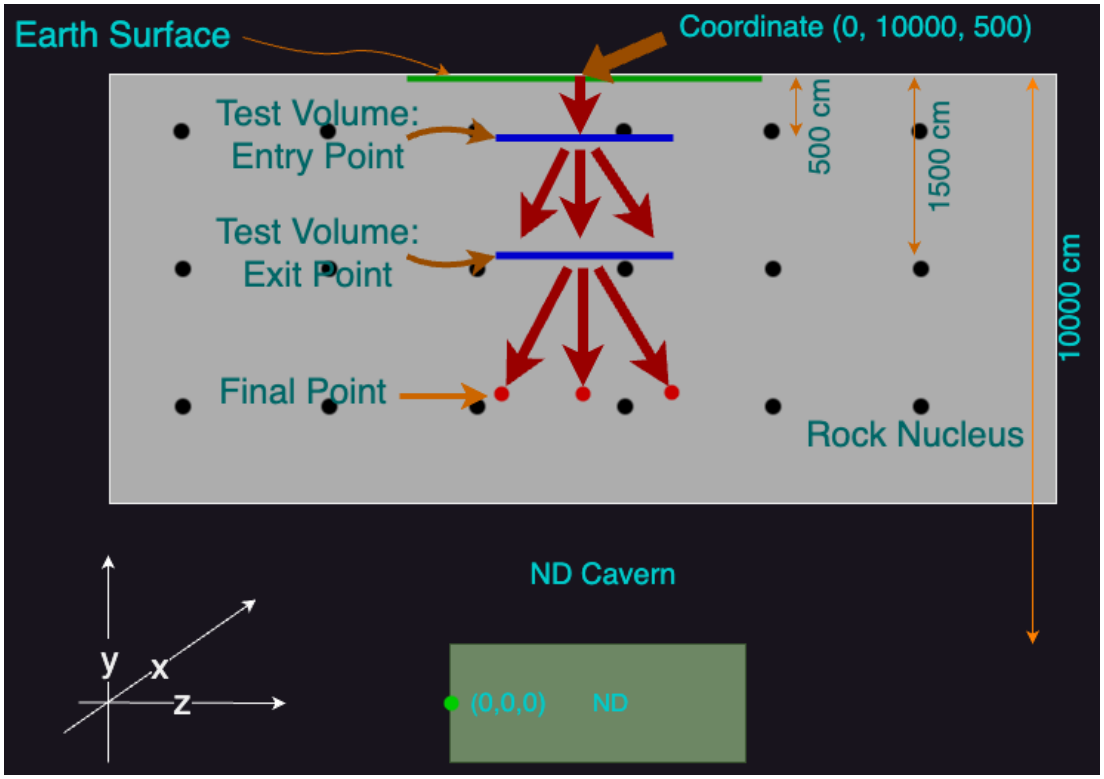

Figure 5.2: GEANT4 environment. 3000 muons propagating through NOvA rock region, starting from earth surface at coordinate (0, 10000, 500) toward ND. The "Entry Point" and "Exit Point" is implemented to calculate the scattering angle on flight.

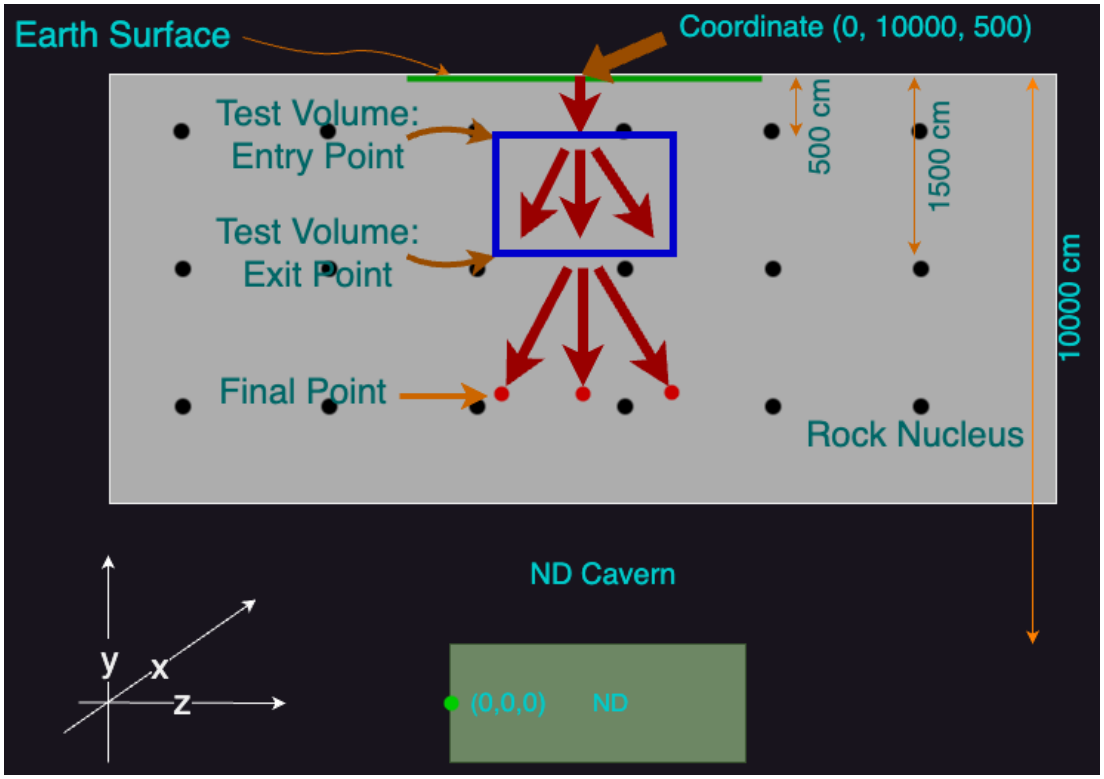

Figure 5.3: PROPOSAL environment. 3000 muons propagating through NOvA rock region, starting from earth surface at coordinate (0, 10000, 500) toward ND. The "Entry Point" and "Exit Point" is depicting the level of the upper and lower boundary of a geometry to calculate the scattering angle on flight. PROPOSAL environment is different from GEANT4 environment only by the implementation of a geometry to calculate scattering angle in mid flight, instead of declaring some cut-off line in GEANT4.

5.2.2 Error Calculation and Validation Test

The error on each data point is calculated with

$$\textbf{error} = \sqrt{N} \quad \text{where } N \text{ is number of entries in each bin} \tag{5.2}$$

The percent difference is calculated for the individual distributions to measure the difference between them using equation:

$$\textbf{percent difference} = \frac{\text{GEANT4 data} - \text{PROPOSAL data}}{\text{GEANT4 data}} \tag{5.3}$$

Error in percent difference is calculated using the division formula of error propagation since **percent difference** is a ratio [26].

$$\frac{\Delta z}{z} = \sqrt{\left(\frac{\Delta x}{x}\right)^2 + \left(\frac{\Delta y}{y}\right)^2} \tag{5.4}$$

where Δz = **Uncertainty in Percent Difference**, z = **percent difference** = $\frac{x}{y}$, x = **GEANT4 data – PROPOSAL data**, and y = **GEANT4 data**. Δx, Δy are error in x and y respectively.

5.2.3 Propagated Distance Validation:

The resulting Propagated Distance validation data are presented from figure 5.4 to 5.7. Each figure shows the distribution comparison for each energy in {3,7,10,40} GeV.

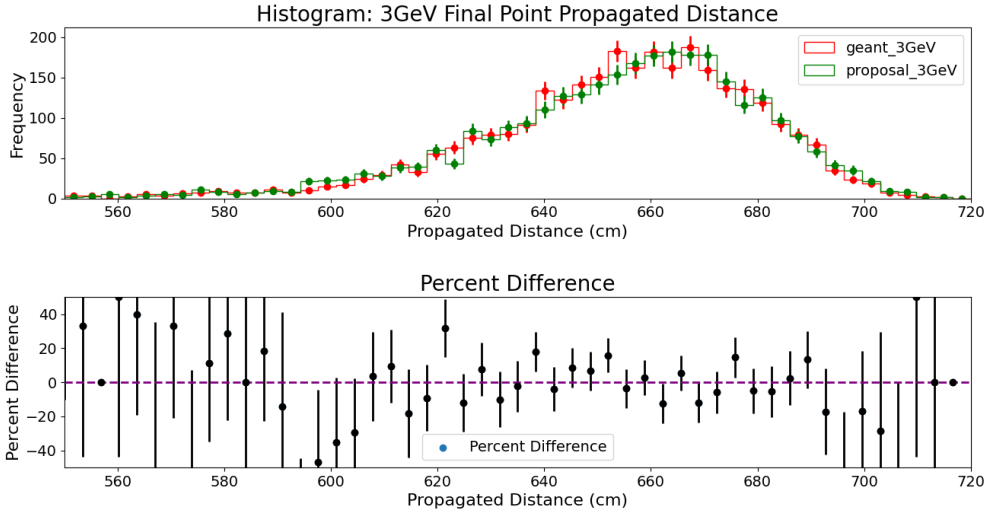

Figure 5.4: Propagated distance distribution for 3GeV muons in GEANT4 (red curve) and PROPOSAL (green curve). Error in distribution plot is calculated using equation 5.2. Percent difference in the bottom plot is calculated using equation 5.3 and uncertainty is calculate by equation 5.4

.

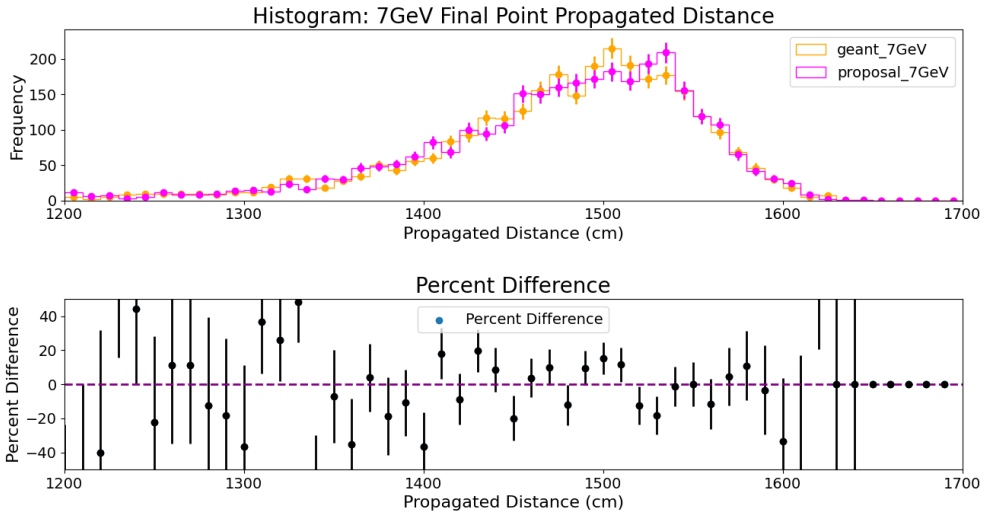

Figure 5.5: Propagated distance distribution for 7GeV muons in GEANT4 (brown curve) and PROPOSAL (magenta curve). Error in distribution plot is calculated using equation 5.2. Percent difference in the bottom plot is calculated using equation 5.3 and uncertainty is calculate by equation 5.4

.

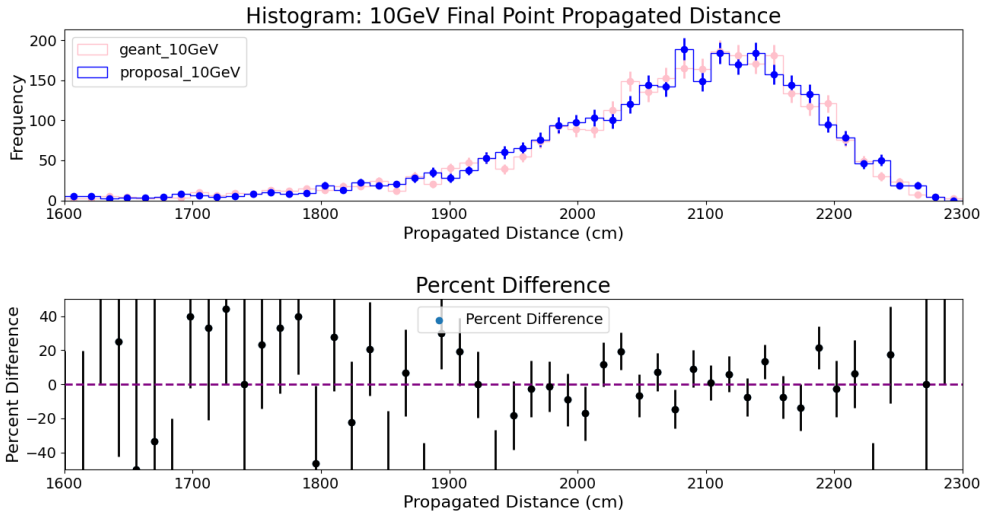

Figure 5.6: Propagated distance distribution for 10GeV muons in GEANT4 (pink curve) and PROPOSAL (blue curve). Error in distribution plot is calculated using equation 5.2. Percent difference in the bottom plot is calculated using equation 5.3 and uncertainty is calculate by equation 5.4

.

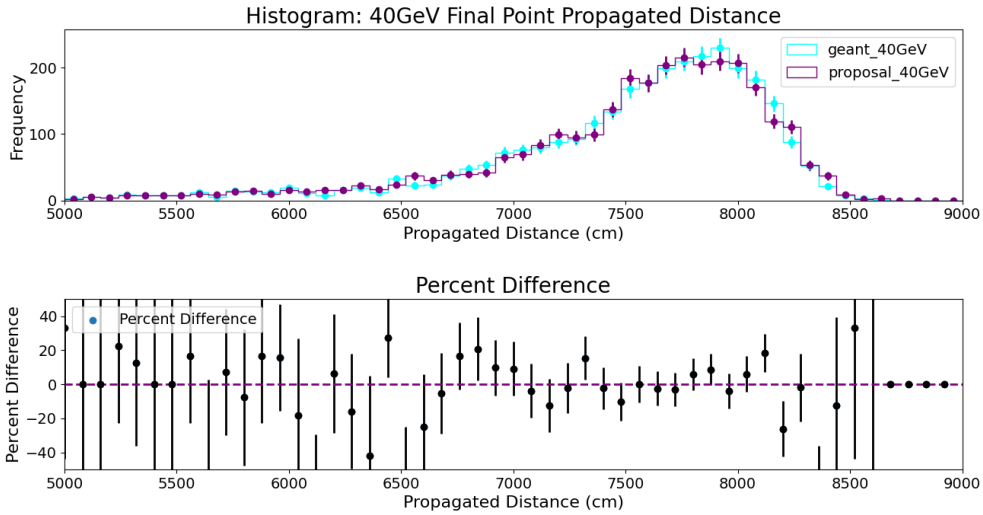

Figure 5.7: Propagated distance distribution for 40GeV muons in GEANT4 (cyan curve) and PROPOSAL (purple curve). Error in distribution plot is calculated using equation 5.2. Percent difference in the bottom plot is calculated using equation 5.3 and uncertainty is calculate by equation 5.4

.

5.2.4 Scattering Angle Validation:

Similarly Scattering Angle validation data are presented in figure 5.8 to 5.11. Each figure shows the scattering angle distribution comparison for each energy in {3,7,10,40}.

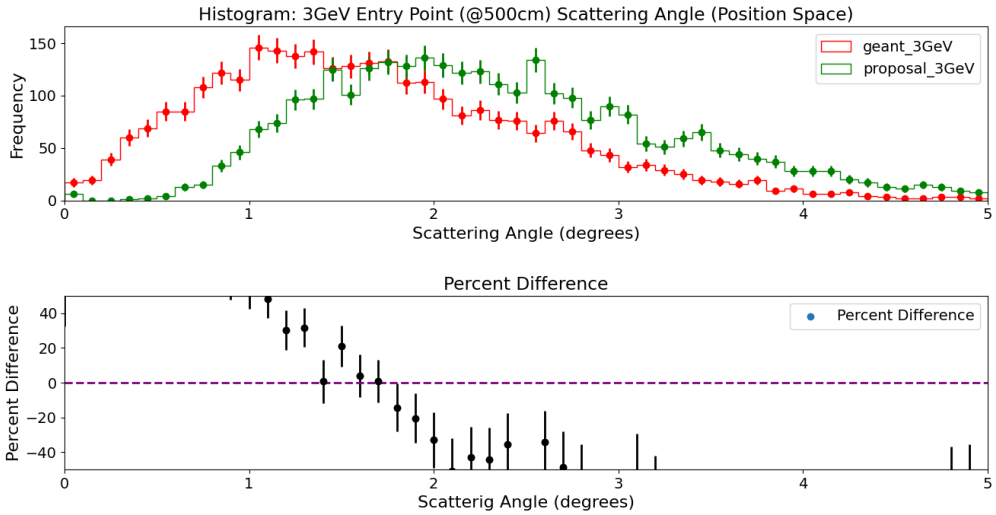

Figure 5.8: Scattering angle distribution for 3GeV muons in GEANT4 (red curve) and PROPOSAL (green curve). Error in distribution plot is calculated using equation 5.2. Percent difference in the bottom plot is calculated using equation 5.3 and uncertainty is calculate by equation 5.4

.

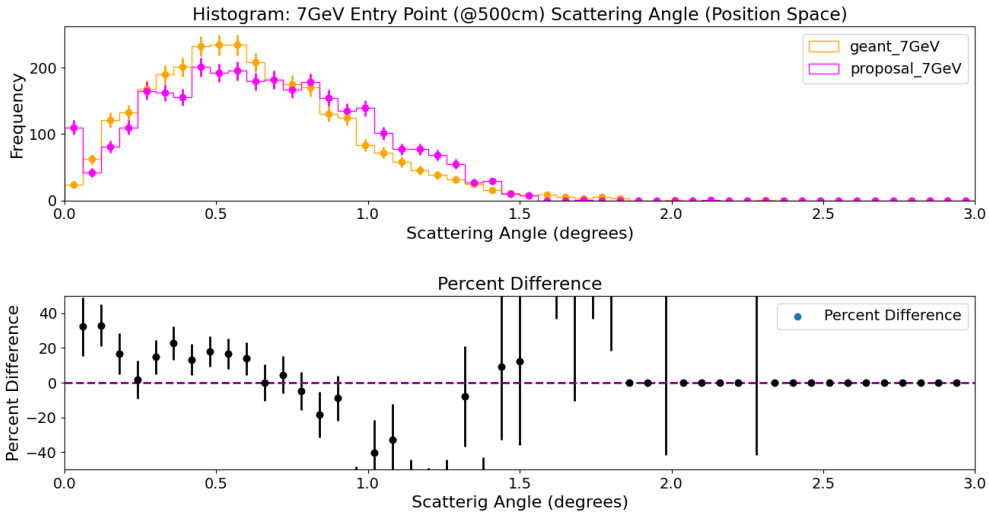

Figure 5.9: Scattering angle distribution for 7GeV muons in GEANT4 (brown curve) and PROPOSAL (magenta curve). Error in distribution plot is calculated using equation 5.2. Percent difference in the bottom plot is calculated using equation 5.3 and uncertainty is calculate by equation 5.4

.

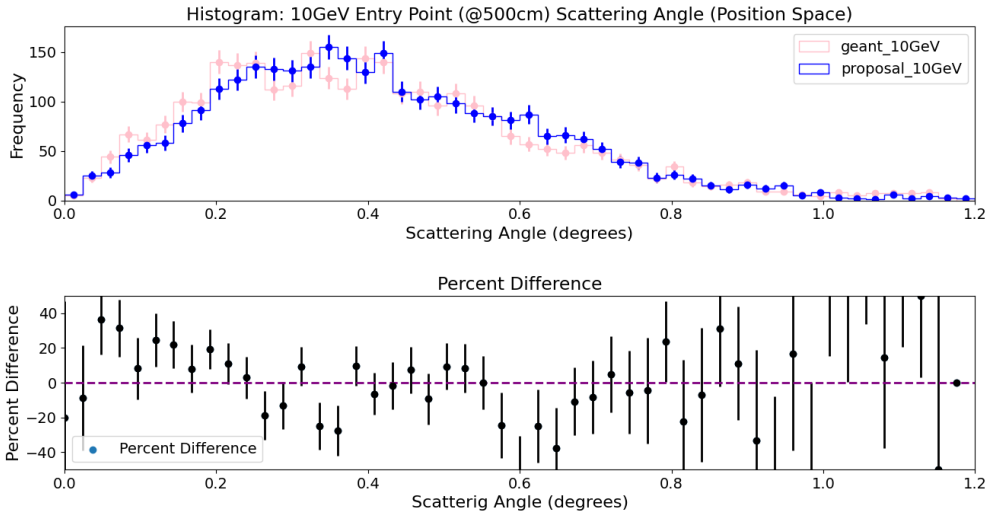

Figure 5.10: Scattering angle distribution for 10GeV muons in GEANT4 (pink curve) and PROPOSAL (blue curve). Error in distribution plot is calculated using equation 5.2. Percent difference in the bottom plot is calculated using equation 5.3 and uncertainty is calculate by equation 5.4

.

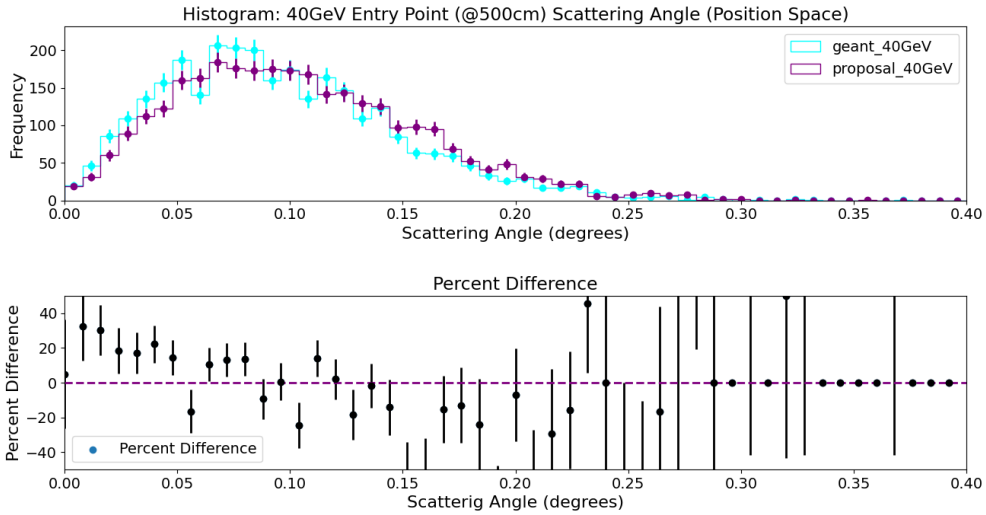

Figure 5.11: Scattering angle distribution for 3GeV muons in GEANT4 (cyan curve) and PROPOSAL (purple curve). Error in distribution plot is calculated using equation 5.2. Percent difference in the bottom plot is calculated using equation 5.3 and uncertainty is calculate by equation 5.4

.

5.2.5 Conclusion:

Percent difference plots show us the state of agreement between two distribution. For **Propagated Distance** plots, we see the shape of both curve is approximately same. For example, in 3 GeV case, all the data points are from both distribution is superimposing each other. In the corresponding percent difference plot, for "**Body Region**" ranging from $\approx [620, 690]$, percent difference values are clumped up near the "**Zero Line**" (purple colored line). On the other hand, percent difference in **Tail Region** ranging from $\approx [0, 620]$ and $\approx [690, 720]$ are located relatively further away from the **Zero line** with high uncertainty. But the uncertainty **prongs** are typically crossing or almost touching the **Zero Line**. Therefore we conclude that the propagated distance distributions for 3 GeV muons are in high agreement. Similar conclusions can be drawn for other propagated distance distributions.

Both models, PROPOSAL and GEANT4, provide similar results when it comes to

how muons propagate through rock medium. However there might be some subtle differences between the results obtained from PROPOSAL and GEANT4 that we might be unable to reliably detect, based on the limited statistical data we worked with. With a larger sample size more significant difference may emerge. Therefore it is necessary to conduct these validations with high statistics.

On the other hand, the scattering angle plots shows a lot of disagreement between them. The 3 GeV case is most prominently disagreed plot among all four cases. In our current understanding, we are unable to provide any valid reason for this high degree of disagreement. But we speculate that PROPOSAL can be handling low energy cases a bit differently than the high energy cases such that the difference in algorithm affects more to scattering angle than the energy loss, i.e., propagated distance calculations. For 7, 10 and 40 GeV cases shows better agreement respectively. **Tail Regions** show greater value for percent difference with long **prongs** of uncertainty that typically crossing or touching the **Zero Line**. The **Body Regions** have percent difference values near to **Zero Line** with small uncertainty. We conclude that for high energy scattering angle cases, both distributions agree which can be improved with higher statistics. However for low energy scattering angle, we need to further investigate.

5.3 Transporting Cosmic Muons by Handling HEP EVT Format File

I collaborated with another fellow NOvA graduate student Amit Pal from National Institute of Science Education and Research, India. For his work on "Seasonal Variation in Cosmic Muons", he needs to perform cosmic muon simulation starting from the upper atmosphere to the near detector. For this purpose, he uses CORSIKA [27] air shower simulation toolkit to

1. propagate the muons from upper atmosphere to earth surface,
2. and then he could do either rock simulation using GEANT4 or simply calculate the straight line trajectory from muon initial state (at earth surface) to final state (at detector surface) considering the geometry, density and other relevant feature of propagation media.

Since the number of particle for Amit's work is huge ($\approx$ 50000), it would consume a lot of computational time to simulate these particle using GEANT4. So, he transports the particles deterministically without considering any statistical nature of the propagation. Since PROPOSAL can propagate particles with 2 order of magnitude faster then GEANT4 and employ statistical features to the simulation, I helped him by propagating those particles using PROPOSAL for rock simulation.

My objective is to take the CORSIKA generated output file as my simulations input and then generate the output file for those particles which will go inside the ND cavern. Instead of propagating till Near Detector (ND), we choose to stop at ND cavern, since inside the ND cavern and ND, we need higher accuracy for simulation, which can be taken care of by GEANT4.

CORSIKA generated files contains mostly muons, antimuons and some protons, neutrons (roughly total 20 proton, neutron among 50000 particles that survives till the earth surface). Since PROPOSAL is a lepton propagator, we want to simulate only muons and antimuons. For that I had to filter out particles other then muons and antimuons and then propagate the leftovers to the ND cavern. Also muons and antimuons are the only particles that are energetic enough to get through the rock to penetrate ND.

The file format for the input/output file is HEP EVT (High Energy Physics Event data) format. HEP EVT file format is a common file format used in high energy physics (HEP) experiments to store event data. Generally HEP experiments generate vast amounts of data, and EVT files are used to store information about individual events, including the particles produced, their properties (such as momentum and energy), and the detector responses to those particles. Figure 5.12 is the image for the first few lines of the HEP EVT input file that I worked on:

```
0 1
1 -13 0 0 0 0 -8.86403 -59.1406 16.8625 62.1332 0.10566 -2015.47 11200 -2802.96 21799.7
1 6
1 -13 0 0 0 0 -0.095317 -93.549 25.7114 97.0181 0.10566 4188.76 11200 -3129.61 46577
1 -13 0 0 0 0 -0.314481 -66.5577 18.1949 69.0007 0.10566 -4020.57 11200 2363.1 27483.1
1 13 0 0 0 0 -0.421117 -73.2284 20.4302 76.0262 0.10566 -5024.5 11200 6187.63 47386.5
1 13 0 0 0 0 -1.13417 -156.962 43.2181 162.807 0.10566 -7427.56 11200 1710.43 21766.1
1 -13 0 0 0 0 -0.158091 -66.3463 17.9658 68.736 0.10566 -1148.57 11200 -489.455 24237.5
1 13 0 0 0 0 -1.42168 -458.16 127.324 475.525 0.10566 -3601.72 11200 8351.38 21018.4
2 1
1 -13 0 0 0 0 -21.9084 -175.127 -55.5863 185.039 0.10566 -1890.25 11200 2311.36 7721.33
```

Figure 5.12: First few lines of the input file for rock simulation. The file is in HEP EVT format

The data structure for this format is following (first 2 lines are described):

Line 1:

$0 \equiv$ Event Number,

$1 \equiv$ Number of particles in this event

Line 2:

$1 \equiv$ number of particle described in this line,

$13 \equiv$ particle pdg number,

$0, 0, 0, 0 \equiv$ 1st mother, 2nd mother, 1st daughter, 2nd daughter particles respectively,

$-8.86403, -59.1406, 16.8625 \equiv$ x, y, z component of momentum respectively (in GeV/c),

$62.1332 \equiv$ energy in GeV,

$0.10566 \equiv$ rest mass in GeV/c^2,

$-2015.47, 11200, -2802.96 \equiv$ x, y, z position coordinate in cm,

$21799.7 \equiv$ time stamp.

Geometry For this simulation, I created 3 geometries,

1. **World Geometry:** This is the background geometry that will hold the simulation. No particles can cross this geometry, otherwise the program will show error. I chose a cubic box of X,Y,Z length $(10^{18} \times 10^{18} \times 10^{18})$ cm^3 and setting the center of this geometry (0, 0, 0) as the origin of my experiment's coordinate system. Density is 1.0 for air.

```
world_geometry = pp.geometry.Box(pp.Cartesian3D(0,0,0), 1E18, 1E18, 1E18)
density_distr_world = pp.density_distribution.density_homogeneous(1.0)
```

2. **Rock Geometry:** The ND rock volume is described in this geometry. Volume $= (10900 \times 10900 \times 10900)$ cm^3 with center at (0, 5000, 0). PROPOSAL considers X as width, Y as height and Z as length. Density value 2.43 for accounting rock density [28].

```
rock_geometry = pp.geometry.Box(pp.Cartesian3D(0,5000,0), 10900, 10900, 10900)
density_distr_rock = pp.density_distribution.density_homogeneous(2.43)
```

3. **ND Cavern Enclosure**: I am considering an imaginary enclosure volume for ND cavern with dimension $900 \times 900 \times 900$ cm^3 with center at (0, 0, 0) and density 1.0 . Instead of taking the exact dimension of ND cavern, we chose to consider an enclosure volume for ND cavern, so that the GEANT4 simulation can take over starting from ND cavern.

```
ndce = pp.geometry.Box(pp.Cartesian3D(0,0,0), 900, 900, 900)
density_distr_ndce = pp.density_distribution.density_homogeneous(1.0)
```

The output file generated by PROPOSAL is shown below:

```
92 1
1 -13 0 0 0 0 14.54197 -103.63589 -36.26428 110.75638 0.10566 -366.46271
450.00000 -125.87154 18121.4
643 1
1 -13 0 0 0 0 -11.45949 -42.32452 -1.61424 43.87826 0.10566 261.63422 450.00000
206.24261 3577.1
670 1
1 13 0 0 0 0 3.41107 -58.98752 -23.51547 63.59364 0.10566 -273.46776 450.00000
93.07566 46859.9
917 1
1 -13 0 0 0 0 -1.24901 -71.63928 -18.66081 74.04042 0.10566 291.14754 450.00000
449.72796 7196.0
1233 1
1 -13 0 0 0 0 2.66280 -94.66984 17.52317 96.31481 0.10566 -370.17751 450.00000 -
446.11997 45713.9
1291 1
1 13 0 0 0 0 -1.96743 -101.76778 -33.37230 107.11803 0.10566 -49.60255 -26.68032
450.00000 35454.6
```

Figure 5.13: Output file generated by PROPOSAL. This file describes the final states for the particles at the ND cavern enclosure boundary.

The output file keeps the event number from the input file the same so that we can know which particle state from the input is hitting the ND cavern enclosure boundary. For example, the first line indicates that the antimuon (-13) state from event number 92 is penetrating through the ND cavern enclosure and the final state of that particle is described in the subsequent line.

5.4 Analysis for Secondary Particles

As charged muons pass through rock, it creates secondary particles as a consequence of interactions between them. These secondary particles can also enter into detector region depending on their state. So they are crucial for NOvA ND studies such as Detector Systematic. However, PROPOSAL does not simulate any particle that is not lepton. And neutrons, protons, gammas and other hadronic particles are constituents of these secondaries. This makes our goal to use PROPOSAL for rock simulation (because its fast) and GEANT4 for ND cavern and ND simulation (because its more accurate). Therefore, we will need to employ strategies to hand the muon simulation from PROPOSAL to GEANT4 at some boundary within the rock but close to the Near Detector. In this regard, we need to decide, at what distance from the ND

cavern, PROPOSAL should hand over the simulation task to GEANT4. Now,

- if PROPOSAL propagates particles very close to the ND cavern boundary, then we will be able to get the information about only those secondary particles that are being generated after the hand over process. We will lose all the information about the secondary particles that have originated at higher position in Y axis and have the capability of entering into ND Cavern.
- On the other hand, if we choose a coordinate in Y axis comparatively higher than the cut off boundary, then the number of generated secondary particles will be huge (because there's lot more volume of rock to generate secondaries) and most of them will not be able to overcome the rest of the rock region to enter ND cavern. Therefore it will render the simulation process slow since we have to account all the primaries and secondaries which are not making till the ND cavern.

Hence we need to decide at what distance from ND cavern we want to take the simulation task from PROPOSAL to GEANT4. A schematic diagram for the simulation is shown in figure 5.14:

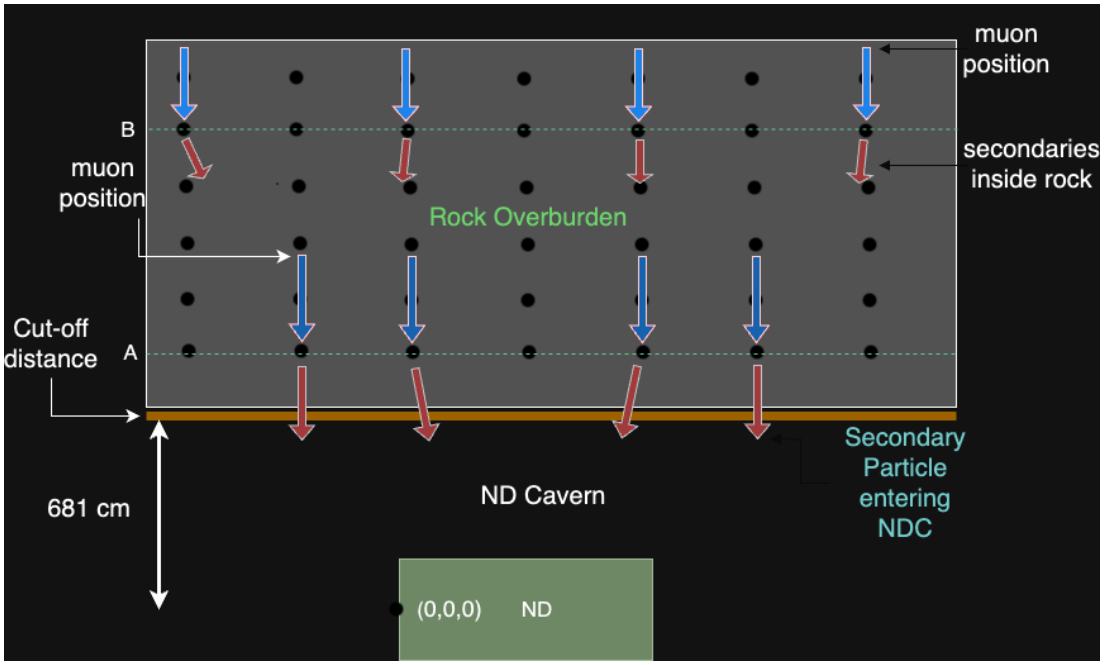

Figure 5.14: A schematic diagram for secondaries analysis. The origin of the coordinate system is set at the center of the XY plane (YZ plane visible) of near detector (ND).Blue and Red arrows depicts the primary muons and secondary particles respectively. File is generated for the particles which passes the ND cavern barrier, i.e. cut-off distance, depicted by the brown colored line. If we choose position "A", we may lose secondary particles originated above "A". If we choose position "B", we will be doing unnecessary simulation for particles most of which will die inside the rock.

The black dots are depicting the rock nucleus inside the "Rock Overburden" region. As the primary muons interacts with the rock nucleus by Bremsstrahlung and Photo Nuclear interaction, it generates secondary gammas, neutrons, etc. We are interested for those secondary particles which are capable of entering into ND cavern.

This experiment is performed in GEANT4. First we considered a mono-energetic beam of primary muons starting from above of the cavern boundary. The experiment is performed for mono energetic muons with energy (3, 5, 7, 10, 30) GeV.
Total number of primary muons is 3000.
Distances from which the primary muons were fired (I call this Primary Muon Location) is following:

- 3GeV: [690, 750, 850, 1000, 1100, 1150, 1200, 1250, 1300, 1350, 1400, 1450, 1500, 1550] cm
- 5GeV: [690, 750, 850, 1000, 1100, 1200, 1300, 1400, 1500, 1600, 1700, 1750, 1800, 1850, 1900, 1950] cm
- 7GeV: [690, 750, 850, 1000, 1100, 1200, 1300, 1400, 1500, 1600, 1700, 1800, 1850, 1900, 1950, 2000, 2050, 2100, 2200, 2300, 2400, 2500] cm
- 10GeV: [690, 750, 850, 1000, 1100, 1200, 1300, 1400, 1500, 1600, 1700, 1800, 1900, 1950, 2000, 2050, 2100, 2200, 2300, 2400, 2500, 2600, 2700, 2800, 2900, 3000] cm
- 30GeV: [690, 850, 1000, 2000, 3000, 4000, 5000, 5500, 5750, 6000, 6250, 6400, 6500, 6600, 6750, 7000, 7250, 7400, 7500, 7600, 7750, 8000] cm

Meaning, say, for 3 GeV muons, 3000 muons were fired from 690 cm, 750 cm, and so on for each distances. And record all the secondary particles that enter ND cavern for each run. Notice that the number of Primary Muon Location is not same for all type of muon energy. This is because, the distance travelled by the primary muon is dependent on its initial energy. For higher initial muon energy, the propagated distance will be longer and hence the probability of producing secondary particles increases. For example, a 3 GeV muon generally travels a track with length 600 cm inside rock. Therefore in order to create secondary particles during 3GeV muons flight, and in order to pass the barrier of cut-off distance (at 681 cm from ND), we placed the Primary Muon Locations starting from 690, 750, 850, .. to 1550 cm. For 30 GeV muon, obviously, this track length is bigger then 600 cm (approximately 7000 cm). Therefore more Primary Muon Locations for 30 GeV than 3 GeV.

After the primary muons are fired to the ND cavern, our program asks the question, how many particles are entering into ND cavern. If they enter, make a file for those secondary particles origin point and calculate its travelled distance to enter into ND cavern. Figure 5.15 is the distribution plot for the secondary particles travelled distance to ND cavern. The two plots shown here are for Gamma and Neutrons as they are the main contributor in total number of secondary particles.

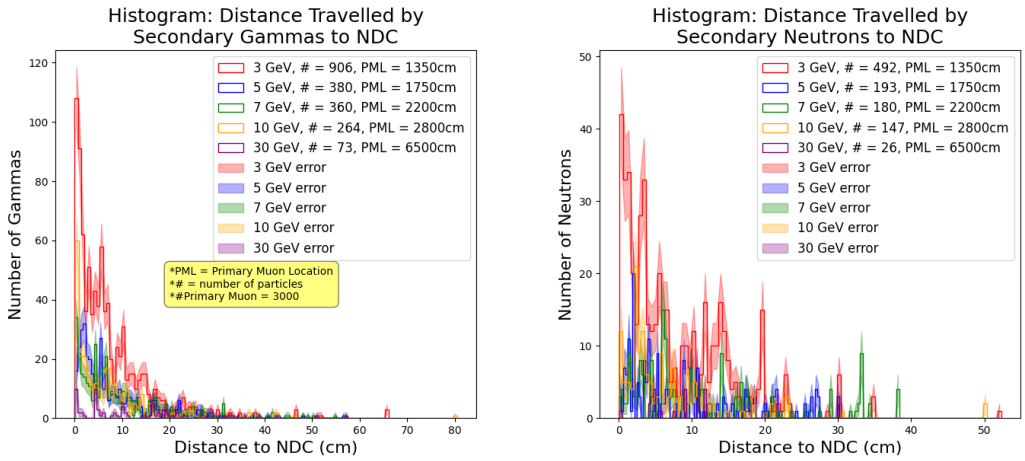

Figure 5.15: Distribution plot for Gamma and Neutrons. The X axis plots the distance in cm for the particle to enter in ND Cavern (NDC). Y axis plots the number of respective particles.

These plots show the distribution for secondary particles generated from different energy. The legend in the plot also tell us the number of particles and "Primary Muon Location" for which the largest number of secondaries have succeeded to enter into ND cavern. For example: "3 GeV, # = 906, PML = 1350cm" tell us that the red curve in the plot is representing the secondary particles originated from the primary muons with energy 3 GeV, and those primary muons were fired from 1350cm above the near detector (the cut-off distance is situated above the near detector at 681 cm, see figure 5.14). The total number of secondary gamma that enters into ND cavern produced by 3 GeV primary muons are 906. Also, the error for all curves are shown by the filled region along the curve. The error is calculated using

$$\textbf{error} = \sqrt{N} \quad \text{where } N \text{ is number of entries in each bin} \tag{5.5}$$

From this plot, we can now decide at what distance the handover process from PROPOSAL to GEANT4 can happen so that we don't lose account for many secondary particles. What percentage of total secondary particles we can neglect, is a question to be decided by the NOvA scientists (Detector Systematic group). Table shows a percentile chart for gamma and neutron distances.

Percentile	Gamma Distance (cm)				
	3 GeV	5 GeV	7 GeV	10 GeV	30 GeV
99	37.93	38.99	48.64	42.04	52.64
95	23.09	25.79	29.56	22.67	35.14
90	16.63	19.78	23.01	15.73	28.32

Table 5.1: Chart for (99, 95, 90) th percentile distance value for secondary Gammas. For example, all the 3 GeV gammas that are plotted in figure 5.15, 99% of those particles traveled distance is within 37.93 cm.

Percentile	Neutron Distance (cm)				
	3 GeV	5 GeV	7 GeV	10 GeV	30 GeV
99	30.18	30.12	38.36	41.19	30.36
95	19.81	26.62	33.30	20.28	25.72
90	16.41	21.62	31.61	12.78	11.8

Table 5.2: Chart for (99, 95, 90) th percentile distance value for secondary Neutrons. For example, all the 3 GeV neutrons that are plotted in figure 5.15, 99% of those particles traveled distance is within 30.18 cm.

For example, if we choose 52.64cm, which is the 99th percentile value for 30 GeV from the chart, we will stop PROPOSAL simulation at $\sim (681 + 52.64 = 733.64)$ and GEANT4 will take over at that position. We can also improve our analysis by filtering out the low energy secondaries by imposing minimum threshold energy value. For example, if the initial energy of the secondary particles are less than "x" MeV, we won't consider them. Because low energy secondaries won't be able to enter into the detector region.

Upon deciding at what distance from ND Cavern we are confident to handover from PROPOSAL to GEANT4, we can define a 3D cut-off geometry in our PROPOSAL code. The purpose of this cut-off geometry will be to tell us if a muon is hitting this

geometry, then we want to consider that muon for our GEANT4 simulation, because that muon and the secondary particles produced by that muon, have a greater chance to enter into ND Cavern and ND. One of the advantage of PROPOSAL is that it can handle defining geometries and particles passing through geometries very easily and efficiently. For example, the following one line of code can provide the state of the particles when they were entering into "PROPOSAL_cut-off_geometry".

```
PROPOSAL_cut-off_geometry_entry_point_state = particles.

entry_point(PROPOSAL_cut-off_geometry)
```

Analysing the "entry_point" states, we can know their energy, momentum (hence direction, hence scattering angle) and deduce if they have greater chance of hitting the detector or not. Figure 5.16 shows a schematic diagram of this process.

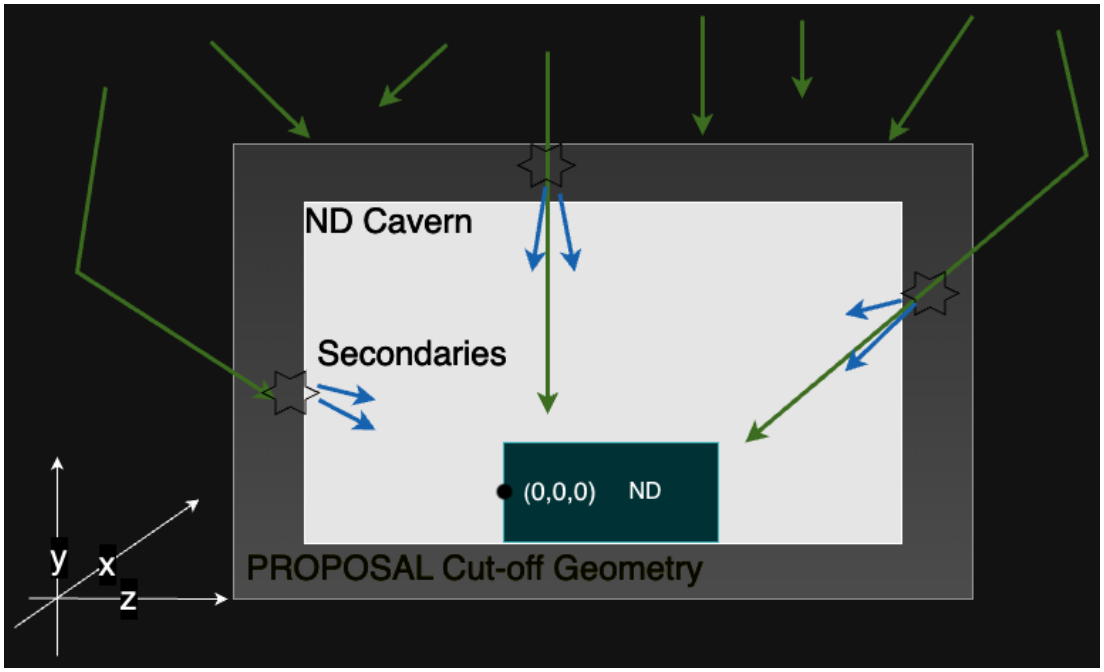

Figure 5.16: A schematic diagram for implementing PROPOSAL cut-off geometry. Muons can from any direction and hit the detector. Therefore we implement PROPOSAL cut-off geometry to tell us which particles are hitting the geometry and which will have greater chance to hit the detector.

Chapter 6

Conclusion and Future Prospect

This thesis focused on validating the PROPOSAL lepton propagation tool by comparing it with the well-established GEANT4 simulation for modeling rock muons in the NOvA experiment. The main objective of this validation study was to evaluate the accuracy and efficiency of PROPOSAL as an alternative simulation tool for simulating muon propagation through the extensive rock volume within the NOvA experiment.

Through a series of careful experiments, we assessed the performance of PROPOSAL by examining crucial parameters, such as the relative energy-cut value for PROPOSAL rock. Our investigation revealed that a relative energy-cut value of 0.007 best aligned with GEANT4 data. We also calculated the $\frac{Z}{A}$ ratio for PROPOSAL rock to be $\frac{10.98}{22.38}$, from this ND rock composition code in NOvA GitHub page [11].

The validation experiments indicated good agreement in the propagated distance distributions. However, there were discrepancies in the low energy scattering angle distributions, with the high energy cases showing better agreement but still not as satisfactory as the propagated distance distributions. As a result, we can conclude that the **Scattering Angle** distributions between PROPOSAL and GEANT4 do not exhibit satisfactory agreement. To gain a deeper understanding of the reason behind this discrepancy, further investigation using additional data is required for a comprehensive analysis.

In Chapter 1, we discussed how our neutrino beam is contaminated by charged

particles like muons. Muons produced by beam neutrinos interacting with rock nucleus can

$$\nu_\mu + N \rightarrow \mu^- + p$$

can enter into detector regions. Understanding the beam energy and constituent profile is crucial for our experiment and therefore the high necessity for muon simulation. While the current simulation tool GEANT4 offers precision in this task, it comes with significant computational overhead. Herein lies the importance of PROPOSAL. PROPOSAL promises to provide efficient and reliable muon simulation, complementing GEANT4's capabilities.

Within the NOvA simulation chain, various tools play pivotal roles. The neutrino event generator program GENIE [29], a Monte Carlo simulation tool, is tasked with handling all aspects of neutrino generation, interactions, and secondary products. Alongside GENIE, GEANT4 and CORSICA also contribute to the simulation process. The ART Event Processing Framework [30] orchestrates these simulation tools, facilitating seamless communication and efficient management. However, integrating PROPOSAL into the ART framework presents technical challenges that are currently being addressed. Overcoming these challenges is crucial for enabling the utilization of GENIE data as input for PROPOSAL and obtaining meaningful output. Despite these obstacles, the validation and analyses presented in this work remain important, as they will inform and guide the implementation of PROPOSAL within NOvA's simulation chain, propelling our studies forward.

We implemented PROPOSAL right away to a more practical case of cosmic muon transportation for NOvA Near Detector. Instead of deterministically calculate final state of muons for rock transportation OR simulating them using GEANT4 with the expense of huge amount of time, we can now use PROPOSAL to handle the problem efficiently and quickly with more realistically by incorporating statistical nature of simulation. We conducted this experiment by taking HEP EVT format file as input and output, which makes the code more universal to use.

Furthermore, we explored the analysis for determining the simulation task handover

process. Since PROPOSAL is fast and GEANT4 is more accurate, we want to use PROPOSAL for rock simulation (sacrificing accuracy but gaining speed) and GEANT4 for detector simulation (sacrificing speed but gaining accuracy). Therefore we need to determine at which point the simulation task should be handover from PROPOSAL to GEANT4. Our "Secondaries" analysis serves that purpose by analysing the secondary particles generated by the transported muons inside the rock. We plotted the 'propagated distance to enter detector region (specifically detector cavern)' distribution for those secondaries for different values of energy for parent muons starting from various altitude. Necessary percentile table has also been prescribed to help make the decision of at what distance handover process should happen.

However, several avenues can be explored to further enhance and refine the results obtained in this thesis, focusing on all the above mentioned results and conclusions.

- **Number of Validation:** To validate PROPOSAL, we presented only two validation parameters (Propagation Distance, Scattering Angle) in this thesis. These are important and essential parameters but we should explore and include new validation parameters like scattering angle in momentum space (to see if both type of scattering angle results is coherent or not), time distribution, etc.

- **More Data:** The validation experiments has been done for 3000 mono-energetic muons of {3,7,10,40} GeV energy to propagate through rock volume. To make the experiment more robust and conclusive, we need to consider more statistics ($\# > 3000$) and more energy-wise explorations.

- **Statistical Methods:** To validate and to measure the disagreement between the distributions, I calculated the percent difference between the distributions. Recently I have come to know about advanced statistical method for comparison between multiple distributions, such as *Chi Square test*, *Anderson-Darling test*, which can be applied to our distributions.

- **3D Secondaries Analysis:** The preliminary "Secondaries" analysis has been performed. However, we need to redo the analysis imposing a minimum threshold energy value for the secondaries. This step is necessary because not all secondaries that enter the cavern will be capable of entering the detector with enough energy to generate detectable scintillation light. We will establish a minimum threshold

energy for the initial energies of the secondaries, selecting only those that have the potential to be detected by the detector. Subsequently, we will validate the effectiveness of PROPOSAL's 3D geometry implementation in determining whether a particle will hit the detector cavern and the detector itself.

References

[1] Sea Agostinelli, John Allison, K al Amako, John Apostolakis, H Araujo, Pedro Arce, Makoto Asai, D Axen, Swagato Banerjee, GJNI Barrand, et al. GEANT4—a simulation toolkit. *Nuclear instruments and methods in physics research section A: Accelerators, Spectrometers, Detectors and Associated Equipment*, 506(3):250–303, 2003.

[2] Mario Dunsch, Jan Soedingrekso, Alexander Sandrock, Max Meier, Thorben Menne, and Wolfgang Rhode. Recent improvements for the lepton propagator proposal. *Computer Physics Communications*, 242:132–144, 2019.

[3] David Griffiths. *Introduction to elementary particles*. John Wiley & Sons, 2020.

[4] Bruno Pontecorvo. Mesonium and antimesonium. *Soviet Journal of Experimental and Theoretical Physics*, 6:429, 1958.

[5] Pn Adamson, K Anderson, M Andrews, R Andrews, I Anghel, D Augustine, A Aurisano, S Avvakumov, DS Ayres, B Baller, et al. The NuMI neutrino beam. *Nuclear Instruments and Methods in Physics Research Section A: Accelerators, Spectrometers, Detectors and Associated Equipment*, 806:279–306, 2016.

[6] DS Ayres, GR Drake, MC Goodman, JJ Grudzinski, VJ Guarino, RL Talaga, A Zhao, P Stamoulis, E Stiliaris, G Tzanakos, et al. The NOvA technical design report. Technical report, Fermi National Accelerator Lab.(FNAL), Batavia, IL (United States), 2007.

[7] Alec Habig. Current results from the noa experiment. July 4, 2023.

[8] NOvA Production Group. Time estimates. Accessed: 2023-07-01.

[9] Donald E Groom and SR Klein. Passage of particles through matter. *The European Physical Journal C-Particles and Fields*, 15(1-4):163–173, 2000.

[10] William R Leo. *Techniques for nuclear and particle physics experiments: a how-to approach; Chapter 2; 2nd ed.* Springer, Berlin, 1994.

[11] Matthew Strait. Nd rock composition. https://github.com/novaexperiment/novasoft/blob/188e4ea9856a6b74e56dc55e82d5759606f05ed6/Geometry/gdml/compositions/ndrock.py#L114.

[12] RM Sternheimer, MJ Berger, and Stephen M Seltzer. Density effect for the ionization loss of charged particles in various substances. *Atomic Data and Nuclear Data Tables*, 30(2):261–271, 1984.

[13] Helmut Paul. Bragg curve. https://upload.wikimedia.org/wikipedia/commons/d/df/Bragg_Curve_for_Alphas_in_Air.png, 2006. Accessed: 2023-06-01.

[14] Wikipedia. Bremsstrahlung. https://en.wikipedia.org/wiki/Bremsstrahlung. Accessed: 2023-06-29.

[15] HW Koch and JW Motz. Bremsstrahlung cross-section formulas and related data. *Reviews of modern physics*, 31(4):920, 1959.

[16] Llewellyn H Thomas. The calculation of atomic fields. In *Mathematical proceedings of the Cambridge philosophical society*, volume 23, pages 542–548. Cambridge University Press, 1927.

[17] Yung-Su Tsai. Pair production and bremsstrahlung of charged leptons. *Reviews of Modern Physics*, 46(4):815, 1974.

[18] Handel Davies, HA Bethe, and LC Maximon. Theory of bremsstrahlung and pair production. ii. integral cross section for pair production. *Physical Review*, 93(4):788, 1954.

[19] GEANT4 Documentation. Pair production by fast muons. https://geant4-userdoc.web.cern.ch/UsersGuides/PhysicsReferenceManual/html/electromagnetic/muon_incident/pair.html. Accessed: 2023-06-29.

[20] J-H Koehne, Katharina Frantzen, Martin Schmitz, Tomasz Fuchs, Wolfgang Rhode, Dmitry Chirkin, and J Becker Tjus. Proposal: A tool for propagation of charged leptons. *Computer Physics Communications*, 184(9):2070–2090, 2013.

[21] GEANT4 Documentation. Pair production by fast muons. https://geant4-userdoc.web.cern.ch/UsersGuides/PhysicsReferenceManual/html/electromagnetic/muon_incident/munu.html. Accessed: 2023-06-29.

[22] GEANT4 Collaboration. Introduction to geant4. https://geant4-userdoc.web.cern.ch/UsersGuides/IntroductionToGEANT4/fo/IntroductionToGEANT4.pdf. Accessed: 2023-06-29.

[23] Makoto Asai. Introduction to geant4. https://cds.cern.ch/record/491492/files/p107.pdf, 2000.

[24] CERN Anton Lechner. Interacting with the geant4 kernel. https://www.ge.infn.it/geant4/training/ornl_2008/retrievinginformationfromkernel.pdf. Accessed: 2023-06-29.

[25] Jean-Marco Alameddine. Simulation of rare processes and electromagnetic shower components within the monte carlo propagation library proposal. https://github.com/Jean1995/Masterarbeit, 2020. Accessed: 2023-06-29.

[26] Statistics How to. Error propagation (propagation of uncertainty). https://www.statisticshowto.com/statistics-basics/error-propagation/. Accessed: 2023-06-29.

[27] D. Heck, J. Knapp, J. N. Capdevielle, G. Schatz, and T. Thouw. CORSIKA: A monte carlo code to simulate extensive air showers. *FZKA Scientific Report*, (6019):1–193, 1998.

[28] Susan Kasahara. Cosmic ray muon simulation to the minos near detector depth, March 5, 2007.

[29] Costas Andreopoulos, Christopher Barry, Steve Dytman, Hugh Gallagher, Tomasz Golan, Robert Hatcher, Gabriel Perdue, and Julia Yarba. The genie neutrino monte carlo generator: physics and user manual. *arXiv preprint arXiv:1510.05494*, 2015.

[30] R Kutschke, M Paterno, and M Wang. Intensity frontier common offline documentation: art workbook and users guide, 2016.

[31] SR Kelner, RP Kokoulin, and AA Petrukhin. Pre-print of moscow engineering physics inst, 1995.

[32] Peter KF Grieder. Cosmic ray muons. In *Cosmic Ray Muography*, pages 33–84. 2023.

[33] Rostislav Pavlovich Kokoulin and Anatoly Afanasievich Petrukhin. Influence of the nuclear form factor on the cross section of electron pair production by high energy muons. In *pp 2436-45 of 12th International Conference on Cosmic Rays. Vol. 6. Hobart, Australia International Union of Pure and Applied Physics (1971).* Inst. of Engineering-Physics, Moscow, 1971.

[34] C Castagnoli, A Castellina, O Saavedra, TM Kirina, RP Kokoulin, and AA Petrukhin. Observation of electromagnetic interactions of high energy muons deep underground. *Physical Review D*, 52(5):2673, 1995.

[35] Leonid B Bezrukov and Eh V Bugaev. Nucleon shadowing effects in photon-nucleus interactions. *Yadernaya fizika*, 33(5):1195–1207, 1981.

Appendix

As a simulation package, PROPOSAL may need to set constraints in its description of physical processes. For example, the energy transfer from primary to secondary is needed to be considered as two different energy transfer process, called stochastic and continuous energy loss depending on some energy cut value set by the user. To incorporate these settings, PROPOSAL's description of physical process differs from the equations discussed in chapter 2. Following is the equations that are being implement in PROPOSAL library. See [20] for detail.

{μ is the mass of propagating particle (muon), m_e is mass of electron, E is energy of incident particle (muon), $\nu = vE$ is the energy of secondary particle (knock-on electron for Ionization, photon for Bremsstrahlung, electron pair for pair production, virtual photon for Photonuclear process) where v is the fraction of energy of primary particle that created the secondaries. All other quantities are same discussed in Chapter 2.}

.1 Ionization

$$-\frac{dE}{dx} = Kz^2\frac{Z}{A\beta^2}\left[\frac{1}{2}\ln\left(\frac{2m_e\beta^2\gamma^2\nu_{upper}}{I(Z)^2}\right) - \frac{\beta^2}{2}\left(1+\frac{\nu_{upper}}{\nu_{max}}\right) + \frac{1}{2}\left(\frac{\nu_{upper}}{2E(1+1/\gamma)}\right)^2 - \frac{\delta}{2}\right] \tag{1}$$

where,

- $\nu_{max} = \frac{2m_e(\gamma^2-1)}{1+2\gamma\frac{m_e}{\mu}+\left(\frac{m_e}{\mu}\right)^2}$.

  It is maximum energy that the secondary particle, in this case, the knock out electron can have. This represents same thing as T_{max} in energy loss for ionization

equation 2.1 from our discussion in Chapter 2 Ionization section.

- $\nu_{upper} = \min(\nu_{cut}, \nu_{max})$
  PROPOSAL implements an energy cut value ν_{cut} for secondary particles for every simulation to distinguish between stochastic and continuous energy loss process. Details about this cut setting is discussed on chapter 4. ν_{upper} is the minimum value between ν_{cut} and ν_{max}.

- $\delta = \begin{cases} \delta_0 10^{2(X-X_0)}, & \text{if} X < X_0 \\ c_1 X + c + a(X_1 - X)^m, & \text{if} X_0 \leq X < X_1 \\ c_1 X + c & \text{else} \end{cases}$
  δ is the density correction term, where $X = \log_{10}(\beta\gamma)$ and the constants $\delta_0, X_0, X_1, c_1, c, a$ are specific to medium material whose values for different materials can be found on the table A.6 from this paper [20]

.2 Bremsstrahlung

The Bremsstrahlung cross section can be expressed as the sum of three components: an elastic component and two inelastic components, one associated with atomic interactions and the other with nuclear interactions.

$$\sigma = \sigma_{el} + \Delta\sigma_a^{in} + \sigma_n^{in}$$

In PROPOSAL, a set of certain parametrization techniques, such as Kelner-Kokoulin-Petrukhin (KKP), Andreev–Bezrukov–Bugaev (ABB), Petrukhin–Shestakov (PS) form factor parametrization can be used for calculating elastic bremsstrahlung. Only KKP is discussed here.

$$\sigma_{el}(E, \nu) = \frac{\alpha}{\nu} \left(2Z\frac{m_e}{\mu} r_e\right)^2 \left(\frac{4}{3} - \frac{4}{3}\nu + \nu^2\right) \left[\ln\frac{\mu}{\delta} - \frac{1}{2} - \Delta_a^{el} - \Delta_n^{el}\right] \tag{2}$$

where, E is energy of incident muon, ν is energy of radiated photon, δ is the minimum momentum transfer, and $\Delta_{a,n}^{el}$ are atomic and nuclear form factors with,

$$\Delta_a^{el}(\delta) = \ln\left[1 + \frac{1}{\delta\sqrt{e}BZ^{-1/3}/m_e}\right] \tag{3}$$

$$\Delta_n^{el}(\delta) = \ln\left[\frac{D_n}{1 + \delta(D_n\sqrt{e} - 2)/\mu}\right] \tag{4}$$

where, $D_n = 1.54A^{0.27}$ and B is radiation log constant whose values are given for different materials in the table A.7 on this PROPOSAL paper [20].

The inelastic contribution in Bremsstrahlung cross section is discussed in this paper [31],

.3 Pair Production

$$\Delta\sigma_a^{in}(E,\nu) \approx \frac{\alpha}{\nu}\left(2Z\frac{m_e}{\mu}r_e\right)^2\left(\frac{4}{3} - \frac{4}{3}\nu + \nu^2\right)\Delta_a^{in} \tag{5}$$

with

$$\Delta_a^{in} \approx \frac{1}{Z}\tilde{\Phi}_a^{in}(\delta) \tag{6}$$

where

$$\tilde{\Phi}_a^{in}(\delta) = \ln\left[\frac{\mu/\delta}{\delta\mu/m_e^2 + \sqrt{e}}\right] - \ln\left[1 + \frac{m_e}{\delta\sqrt{e}B'Z^{-2/3}}\right] \tag{7}$$

where, $B' = 1429$ for $Z \geq 2$ and $B' = 446$ for $Z = 1$.
The nuclear contribution can be found similarly by using $\Delta_n^{in} = \frac{1}{Z}\Delta_n^{el}$.

The cross section formulae used in PROPOSAL are from the reference [32, 33, 34]

$$\frac{d\sigma(E,\nu,\rho)}{d\nu d\rho} = \frac{2}{3\pi}Z(Z+\zeta)(\alpha r_e)^2\frac{1-\nu}{\nu}\left(\Phi_e + \frac{m^2}{\mu^2}\Phi_\mu\right) \tag{8}$$

with, $\nu = (\epsilon_+ + \epsilon_-)/E$, $\rho = (\epsilon_+ - \epsilon_-)/E$ where, ϵ_{+-} is positron and electron energy.
Also,

$$\Phi_e = \left\{[(2+\rho^2)(1+\beta)\xi(3+\rho^2)]\ln\left(1 + \frac{1}{\xi}\right) + \frac{1-\rho^2-\beta}{1+\xi} - (3+\rho^2)\right\}L_e \tag{9}$$

$$\Phi_\mu = \left\{\left[(1+\rho^2)(1+\frac{3}{2}\beta) - \frac{1}{\xi}(1+2\beta)(1-\rho^2)\right]\ln(1+\xi) + \frac{\xi(1-\rho^2-\beta)}{1+\xi} + (1+2\beta)(1-\rho^2)\right\}L_\mu \tag{10}$$

$$L_e = \ln\left(\frac{BZ^{-1/3}\sqrt{(1+\xi)(1+Y_e)}}{1+\frac{2m_e\sqrt{e}BZ^{-1/3}(1+\xi)(1+Y_e)}{E\nu(1-\rho^2)}}\right) - \frac{1}{2}\ln\left[1+\left(\frac{3m_e}{2\mu}Z^{1/3}\right)^2(1+\xi)(1+Y_e)\right] \tag{11}$$

$$L_\mu = \ln\left(\frac{\frac{2}{3}\frac{\mu}{m_e}BZ^{-2/3}}{1+\frac{2m_e\sqrt{e}BZ^{-1/3}(1+\xi)(1+Y_e)}{E\nu(1-\rho^2)}}\right) \tag{12}$$

$$Y_e = \frac{5-\rho^2+4\beta(1+\rho^2)}{2(1+3\beta)\ln(3+\frac{1}{\xi})-\rho^2-2\beta(2-\rho^2)} \tag{13}$$

$$Y_\mu = \frac{4+\rho^2+3\beta(1+\rho^2)}{(1+\rho^2)(3/2+2\beta)\ln(3+\xi)+1-\frac{3}{2}\rho^2} \tag{14}$$

$$\beta = \frac{\nu^2}{2(1-\nu)} \tag{15}$$

$$\xi = \left(\frac{\mu\nu}{2m_e}\right)^2\frac{1-\rho^2}{1-\nu} \tag{16}$$

$$\zeta_{loss}^{pair}(E,Z) \approx \frac{0.073\ln\left(\frac{E/\mu}{1+\gamma_1 Z^{2/3}E/\mu}\right)-0.26}{0.058\ln\left(\frac{E/\mu}{1+\gamma_2 Z^{1/3}E/\mu}\right)-0.14} \tag{17}$$

$$\gamma_1 = 1.95\times10^{-5} \text{ and } \gamma_2 = 5.3\times10^{-5} \text{ for } Z\neq 1, \tag{18}$$

$$\gamma_1 = 4.4\times10^{-5} \text{ and } \gamma_2 = 4.8\times10^{-5} \text{ for } Z = 1 \tag{19}$$

.4 Photonuclear Interaction

In PROPOSAL, the Bezrukov-Bugaev Parametrization is used for photonuclear interaction [35]. The underlined terms in the cross section equation are used to account for tau propagation.

$$\frac{d\sigma}{d\nu} = \frac{\alpha}{2\pi} A\sigma_{\gamma N}\nu\,[\mathrm{Term}_1 + \mathrm{Term}_2 + \mathrm{Term}_3] \tag{20}$$

with,

$$\mathrm{Term}_1 = 0.75G(x)\left[k\ln\left(1+\frac{m_1^2}{t}\right) - \frac{km_1^2}{m_1^2+t} - \frac{2\mu^2}{t} + \frac{4\mu^2}{m_1^2\ln\left(1+\frac{m_1^2}{t}\right)}\right]$$

$$\mathrm{Term}_2 = 0.25\left[\left(k+\frac{2\mu^2}{m_2^2}\right)\ln\left(1+\frac{m_2^2}{t}\right) - \frac{2\mu^2}{t}\right]$$

$$\mathrm{Term}_3 = \frac{\mu^2}{2t}\left[0.75G(x)\frac{m_1^2-4t}{m_1^2+t} + 0.25\frac{m_2^2}{t}\ln\left(1+\frac{t}{m_2^2}\right)\right]$$

where,

$t = Q^2_{max} = \frac{\mu^2\nu^2}{1-\nu}$; $\quad k = 1 - \frac{2}{\nu} - \frac{2}{\nu^2}$; $\quad m_1^2 = 0.54GeV^2$ and $m_2^2 = 1.8GeV^2$

Nucleon shadowing effect is accounted with

$\sigma_{\gamma A}(\nu) = A\sigma_{\gamma N}(\nu)\{0.75G(x) + 0.25\}$

with $G(x) = \frac{3}{x^3}\left(\frac{x^2}{2} - 1 + e^{-x}(1+x)\right)$ for $Z \neq 1$;

And $G(x) = 1$ for $Z = 1$, with $x = 0.00282A^{1/3}\sigma_{\gamma N}(\nu)$

$\sigma_{\gamma N}$ refers to the photon nucleon cross section.

The Abramowicz–Levin–Levy–Maor (ALLM) parametrization is also implemented in PROPOSAL for photonuclear cross section. Please see [20] for detailed discussion.